# Postnatal changes of vesicular glutamate transporter (VGluT)1 and VGluT2 immunoreactivities and their colocalization in the mouse forebrain

**ARTICLE** *in* THE JOURNAL OF COMPARATIVE NEUROLOGY · NOVEMBER 2005

Impact Factor: 3.23 · DOI: 10.1002/cne.20705 · Source: PubMed

THE JOURNAL OF COMPARATIVE NEUROLOGY 492:263–288 (2005)

# Postnatal Changes of Vesicular Glutamate Transporter (VGluT)1 and VGluT2 Immunoreactivities and Their Colocalization in the Mouse Forebrain

KOUICHI NAKAMURA,[1] HIROYUKI HIOKI,[1] FUMINO FUJIYAMA,[1] AND TAKESHI KANEKO[1,2]*

[1]Department of Morphological Brain Science, Graduate School of Medicine, Kyoto University, Kyoto 606-8501, Japan

[2]Core Research for Evolutional Science and Technology, Japan Science and Technology Agency, Kawaguchi 332-0012, Japan

ABSTRACT

Vesicular glutamate transporter 1 (VGluT1) and VGluT2 accumulate neurotransmitter glutamate into synaptic vesicles at presynaptic terminals, and their antibodies are thus considered to be a good marker for glutamatergic axon terminals. In the present study, we investigated the postnatal development and maturation of glutamatergic neuronal systems by single- and double-immunolabelings for VGluT1 and VGluT2 in mouse forebrain including the telencephalon and diencephalon. VGluT2 immunoreactivity was widely distributed in the forebrain, particularly in the diencephalon, from postnatal day 0 (P0) to adulthood, suggesting relatively early maturation of VGluT2-loaded glutamatergic axons. In contrast, VGluT1 immunoreactivity was intense only in the limbic regions at P0, and drastically increased in the other telencephalic and diencephalic regions during three postnatal weeks. Interestingly, VGluT1 immunoreactivity was frequently colocalized with VGluT2 immunoreactivity at single axon terminal-like profiles in layer IV of the primary somatosensory area from P5 to P10 and in the ventral posteromedial thalamic nucleus from P0 to P14. This was in sharp contrast to the finding that almost no colocalization was found in glomeruli of the olfactory bulb, patchy regions of the caudate-putamen, and the ventral posterolateral thalamic nucleus, where moderate to intense immunoreactivities for VGluT1 and VGluT2 were intermingled with each other in neuropil during postnatal development. The present results indicate that VGluT2-loaded glutamatergic axons maturate earlier than VGluT1-laden axons in the mouse telencephalic and diencephalic regions, and suggest that VGluT1 plays a transient developmental role in some glutamatergic systems that mainly use VGluT2 in the adulthood. J. Comp. Neurol. 492:263–288, 2005. 

**Indexing terms: glutamatergic neurons; central nervous system; immunohistochemistry; excitatory; double immunofluorescence**

An understanding of the emergence and maturation of glutamatergic neuronal circuitry is an important issue in the field of developmental neuroscience, because glutamate is a major excitatory neurotransmitter that plays a principal role in mammalian central nervous system (CNS). The development of glutamatergic circuitry has been studied morphologically with immunocytochemical and in situ hybridization histochemical probes by localizing key molecules that mediate glutamatergic neurotransmission. For example, many groups have intensively investigated the developmental changes of glutamate receptors (for review, see Herlenius and Lagercrantz, 2004; Luján et al., 2004). However, immunoreactivities and mRNA signals for these glutamate receptors are generally the markers for postsynaptic but not presynaptic elements of glutamatergic systems. Therefore, these in-

Grant sponsor: the Ministry of Education, Science, Sports, and Culture of Japan; Grant number: 16200025; Grant number: 16500217; Grant number: 17022020; Grant number: 17022024; Grant number: 15-5638; Grant sponsor: the Japan Society for the Promotion of Science for Young Scientists (Research Fellowships to K.N.).

*Correspondence to: Takeshi Kaneko, Department of Morphological Brain Science, Graduate School of Medicine, Kyoto University, Kyoto 606-8501, Japan. E-mail: kaneko@mbs.med.kyoto-u.ac.jp

Received 23 April 2005; Revised 7 June 2005; Accepted 13 June 2005

DOI 10.1002/cne.20705

Published online in Wiley InterScience (www.interscience.wiley.com).

vestigations have not provided morphological information on the development of presynaptic glutamatergic components in the CNS. In contrast, immunoreactivity for glutamate has been used in the CNS as a morphological marker for presynaptic glutamatergic components of glutamatergic systems, i.e., glutamatergic neurons and their axon terminals (for review, see Broman et al., 2000; Kaneko, 2000). Glutamate immunoreactivity is, however, not specific to glutamatergic systems, because glutamate is a general metabolic substrate or serves as the precursor of the inhibitory neurotransmitter γ-aminobutyric acid (GABA). Because phosphate-activated glutaminase has been demonstrated to be the principal synthetic enzyme for neurotransmitter glutamate, glutaminase immunoreactivity has been used as a marker for glutamatergic systems (for review, see Kaneko, 2000) and applied to the investigation of developing rat brain (Kaneko and Mizuno, 1992). Although glutaminase immunoreactivity is a specific marker for glutamatergic neurons in the cerebral cortex (Kaneko et al., 1992; Kaneko and Mizuno, 1994), glutaminase is located in some GABAergic neurons in the brain, such as thalamic reticular nucleus neurons and globus pallidus neurons, possibly supplying GABA-precursor glutamate in these neurons (Kaneko and Mizuno, 1988, 1992). Thus, more specific markers are required for the study of presynaptic components of glutamatergic systems.

Vesicular uptake of glutamate is a specific event to glutamatergic axon terminals, because it is a necessary process before neurotransmitter glutamate is released from synaptic vesicles into the synaptic cleft. Recently, three vesicular glutamate transporters (VGluTs) have been identified on a molecular basis (Bellocchio et al., 2000; Takamori et al., 2000, 2001, 2002; Bai et al., 2001; Fremeau et al., 2001, 2002; Herzog et al., 2001; Gras et al., 2002; Schäfer et al., 2002; Varoqui et al., 2002). Immunoelectron-microscopic analyses have revealed that VGluT1 and VGluT2 are located on small round vesicles of axon terminals making asymmetric type of synapses, supporting the hypothesis that they act as vesicular proteins for glutamate uptake (Bellocchio et al., 1998; Fremeau et al., 2001; Fujiyama et al., 2001; Herzog et al., 2001).

*Abbreviations*

| | |
|---|---|
| 1n | olfactory nerve |
| A1 | primary auditory area |
| ABC | avidin-biotin peroxidase complex |
| ac | anterior commissure |
| AD | anterodorsal thalamic nucleus |
| AM | anteromedial thalamic nucleus |
| AOB | accessory olfactory bulb |
| AON | anterior olfactory nucleus |
| APS | 3-aminopropyl triethoxysilane |
| AV | anteroventral thalamic nucleus |
| alv | alveus |
| AM | anteromedial thalamic nucleus |
| Amyg | amygdaloid nuclear complex |
| APS | 3-aminopropyltriethoxysilane |
| APT | anterior pretectal nucleus |
| AV | anteroventral thalamic nucleus |
| BST | bed nucleus of the stria terminalis |
| CA1 | cornu ammonis 1 |
| CA2 | cornu ammonis 2 |
| CA3 | cornu ammonis 3 |
| Cg | cingulate area |
| CL | centrolateral thalamic nucleus |
| CM | central medial thalamic nucleus |
| cp | cerebral peduncle |
| CP | undifferentiated cortical plate |
| CPu | caudate-putamen |
| DG | dentate gyrus |
| Ent | entorhinal area |
| EPL | external plexiform layer |
| f | fornix |
| fr | fasciculus retroflexus |
| GABA | γ-aminobutyric acid |
| Gl | glomerular layer |
| Gr | granule cell layer |
| H | hilar region of the dentate gyrus |
| Hb | habenular nuclei |
| ic | internal capsule |
| IPL | internal plexiform layer |
| iz | intermediate zone |
| LD | laterodorsal thalamic nucleus |
| LGd | dorsal lateral geniculate nucleus |
| LGv | ventral lateral geniculate nucleus |
| LHb | lateral habenular nucleus |
| LM | stratum lacunosum-moleculare of the hippocampus |
| LOT | lateral olfactory tract |
| LP | lateroposterior thalamic nucleus |
| Lu | stratum lucidum of the hippocampus |
| M1 | primary motor area |
| MD | mediodorsal thalamic nucleus |
| MG | medial geniculate nucleus |
| MGd | medial geniculate nucleus, dorsal part |
| MGv | medial geniculate nucleus, ventral part |
| MHb | medial habenular nucleus |
| Mi | mitral cell layer |
| Mm | mammillary nucleus |
| mt | mammillothalamic tract |
| MZ | marginal zone |
| Or | stratum oriens of the hippocampus |
| OT | olfactory tubercle |
| P | postnatal day |
| Pa | paraventricular hypothalamic nucleus |
| PBS | phosphate-buffered saline |
| PBS-X | PBS with 0.3% (v/v) Triton X-100 |
| PBS-XCD | PBS-X containing 0.25% (w/v) λ-carrageenan and 1% (v/v) donkey serum |
| PC | paracentral thalamic nucleus |
| Pir | piriform area |
| Po | posterior thalamic nuclear group |
| PoSub | postsubiculum |
| PT | paratenial thalamic nucleus |
| PV | paraventricular thalamic nucleus |
| Py | stratum pyramidale of the hippocampus |
| Ra | stratum radiatum of the hippocampus |
| Re | reuniens thalamic nucleus |
| RS | retrosplenial area |
| Rt | reticular thalamic nucleus |
| S1 | primary somatosensory area |
| S2 | secondary somatosensory area |
| SC | superior colliculus |
| Sep | septal nuclei |
| sm | stria medullaris of the thalamus |
| Sm | submedius thalamic nucleus |
| SNr | substantia nigra pars reticulata |
| SP | subplate |
| st | stria terminalis |
| TH | tyrosine hydroxylase |
| V1 | primary visual area |
| V2 | secondary visual area |
| VA | ventroanterior thalamic nucleus |
| VGluT | vesicular glutamate transporter |
| VL | ventrolateral thalamic nucleus |
| VM | ventromedial thalamic nucleus |
| VPL | ventral posterolateral thalamic nucleus |
| VPM | ventral posteromedial thalamic nucleus |
| wm | white matter |

Although VGluT1 and VGluT2 show highly similar biochemical and pharmacological properties for glutamate uptake (for review, see Kaneko and Fujiyama, 2002; Fremeau et al., 2004a), the two proteins display a clearly complementary distribution in in situ hybridization histochemistry and immunocytochemistry (Ni et al., 1995; Hisano et al., 2000; Fremeau et al., 2001; Fujiyama et al., 2001; Herzog et al., 2001; Kaneko et al., 2002). VGluT1 is expressed mostly in telencephalic regions, whereas VGluT2 is mainly produced in diencephalic and lower brainstem regions of the adult rodent brain. This indicates that VGluT1 and VGluT2 are principally used by segregated neuronal populations. In contrast to VGluT1- and VGluT2-expressing neurons, VGluT3-expressing neurons constitute a much smaller population in the brain and show chemical characteristics other than those of a glutamatergic nature, such as cholinergic, serotonergic, and GABAergic phenotypes (Fremeau et al., 2002; Fujiyama et al., 2004; Hioki et al., 2004). Thus, mRNA signals or immunoreactivities for VGluT1 and VGluT2 proteins, respectively, can be used as markers for the vast majority of glutamatergic neuronal cell bodies or axon terminals in the CNS.

Several groups recently reported the distribution of VGluT1 and VGluT2 mRNA signals in the postnatal developing mouse brain. Briefly, VGluT2 mRNA expression was high in diencephalic and lower brainstem regions at postnatal day 1 (P1), whereas VGluT1 mRNA expression was high only in limbic regions but low in the other telencephalic regions at P1 (Miyazaki et al., 2003; Fremeau et al., 2004b). VGluT1 mRNA expression in telencephalic regions increased drastically over 2 postnatal weeks. Because the emergence of VGluT proteins at axon terminals is a prerequisite for the functional maturation of presynaptic glutamatergic components, investigation of the distribution of VGluT1 and VGluT2 proteins during postnatal period is crucial for an understanding of excitatory circuit development. Recently, the development of VGluT1 and VGluT2 immunoreactivities in the mouse cerebellum was studied in detail immunocytochemically by Miyazaki et al. (2003), and that in the rat whole brain was reported by Boulland et al. (2004) using immunocytochemical and Western blotting techniques. The results of these immunocytochemical studies were mostly in good agreement with those of in situ hybridization analyses in developing brain.

VGluT1 and VGluT2 proteins, as described above, show a complementary distribution in the mature brain, and their colocalization in single axon terminals has been found only in very limited regions such as mossy fiber terminals in the cerebellar cortex (Hioki et al., 2003). However, recent developmental studies using in situ hybridization histochemistry and VGluT1 knockout mice reported that the two VGluTs were transiently co-expressed in pyramidal cells of the hippocampal CA1 region during the postnatal period; these studies suggested that granule cells of the dentate gyrus and pyramidal neurons of the neocortex may also co-express the two VGluTs transiently in postnatal development (Miyazaki et al., 2003; Fremeau et al., 2004b; Wojcik et al., 2004). These findings made us speculate that the transient co-expression of VGluT1 and VGluT2 might play a role in synapse formation and/or plasticity of excitatory circuitry in the developing forebrain. Thus, in the present study, we attempted to show the postnatal changes in VGluT1 and VGluT2 immunoreactivities and their colocalization in the mouse forebrain (including the telencephalon and diencephalon), by using single- and double-immunolabeling methods.

## MATERIALS AND METHODS

### Animals

The experiments were conducted in accordance with the rules of animal care of the Institute of Laboratory Animals, Graduate School of Medicine, Kyoto University. C57BL/6 mice were purchased from Japan SLC (Shizuoka, Japan). The day of birth was defined as postnatal day 0 (P0). A total of 36 mice of P0, P1, P3, P5, P7, P10, P14, and P22, as well as 12-week-old (adult) were used in the present study. All efforts were made to minimize animal suffering and the number of animals used.

### Fixation and immunoperoxidase staining

Four mice per each age were deeply anesthetized with cooling on ice for P0–P3 mice or sodium pentobarbital (5 mg/100 g body weight) for P5–P22 and adult mice. The mice were perfused transcardially with 2–20 ml (varying with animal size) of 5 mM phosphate-buffered 0.9% (w/v) saline (PBS, pH 7.2), followed by perfusion for 30 minutes with 3–30 ml of 0.1 M sodium phosphate buffer (pH 7.2) containing 4.0% (v/v) formaldehyde. The brains were removed and postfixed at 4°C overnight in the same fixative. After cryoprotection with 30% (w/v) sucrose in PBS, the brains were cut into 50-μm-thick frontal sections on a freezing microtome. Every six sections that were collected in separate bottles were stained for VGluT1 or VGluT2 immunoreactivity. Some unused sections and some immunostained sections were Nissl-stained with cresyl violet to determine the cytoarchitecture.

The sections were incubated overnight with 0.2 μg/ml affinity-purified anti-VGluT1 or 0.5 μg/ml affinity-purified anti-VGluT2 rabbit IgG (Hioki et al., 2003) and then for 1 hour with 1:100 diluted biotinylated anti-(rabbit IgG) donkey antibody (AP182B, Chemicon, Temecula, CA). Antibody incubation was carried out at room temperature in PBS containing 0.3% (v/v) Triton X-100, 0.25% (w/v) λ-carrageenan, and 1% (v/v) donkey serum (PBS-XCD), followed by two washes with PBS containing 0.3% (v/v) Triton X-100 (PBS-X). The sections were further incubated for 1 hour with 1:50 diluted avidin-biotinylated peroxidase complex (ABC; Elite ABC kit, Vector, Burlingame, CA) in PBS-X. After two rinses in PBS, the sections were reacted for 20–40 minutes with 0.02% (w/v) diaminobenzidine-4HCl (Dojindo, Tokyo, Japan) and 0.001% (v/v) $H_2O_2$ in 50 mM Tris-HCl (pH 7.6), mounted onto 3-aminopropyltriethoxysilane (APS)-coated glass slides (Matsunami, Kishiwada, Japan), dehydrated in ethanol series, cleared in xylene, and coverslipped. P22 mouse sections containing regions of internal standards (see Results) for evaluation of immunoreactivity were always processed in the same incubation chamber together with specimens of different postnatal ages. The relative intensity of VGluT immunoreactivity was carefully determined by comparing the stained sections with the internal standard P22 sections.

The anti-VGluT1 and anti-VGluT2 antibodies were produced against C-terminal nonadecapeptides of rat VGluT1 and C-terminal nonacosapeptides of rat VGluT2; the antigen sites were entirely different from each other. These

antibodies have been characterized in adult rat tissue by Western blotting and immunohistochemistry (Fujiyama et al., 2001; Hioki et al., 2003). The antigen peptide sequence for VGluT1 has 100% identity (19/19) with the C-terminal portion of mouse VGluT1, and that for VGluT2 has 93.1% identity (27/29) with the mouse VGluT2 C-terminus. With the absorbed primary antibodies in the presence of 10,000-fold (in mol) excess amount of the antigen peptides or without the primary antibodies, only very low or no background staining was observed, supporting the high specificity of these antibodies in mouse tissue.

All photographs were taken by a digital camera (Penguin Pro 600ES, Pixera, Los Gatos, CA). The digital images were arranged and modified (±30% contrast enhancement) in software Canvas 9 (ACD Systems, Saanichton, BC, Canada) and saved as TIFF files. Cytoarchitectonic areas were determined by using Nissl-stained sections and were based on the atlases of Paxinos and Franklin (2001), Paxinos et al. (1991), and Altman and Bayer (1995).

### Double- and triple-immunofluorescence study

In immunofluorescence staining, we treated the sections of P0–P22 and adult mouse by the antigen retrieval method of Jiao et al. (1999) prior to primary antibody incubation in order to increase the fluorescent signal and avoid underestimation of colocalization (see Discussion). Briefly, the sections were incubated in a tube containing 1 ml of 10 mM sodium-citrate buffer, pH 6.0, at room temperature for 5 minutes and at 80°C for 1 hour, and were then cooled down to room temperature for 30 minutes.

For double-immunofluorescence staining for VGluT1 and VGluT2, the sections were incubated overnight with a mixture of 5 μg/ml anti-VGluT1 guinea pig IgG (Fujiyama et al., 2001) and 5 μg/ml anti-VGluT2 rabbit IgG, overnight with 1:20 diluted biotinylated anti-(rabbit IgG) donkey antibody, and then finally overnight with 10% rabbit serum, 10 μg/ml AlexaFluor 488-conjugated streptavidin (S11223, Molecular Probes, Eugene, OR), and 50 μg/ml Cy5-conjugated anti-(guinea pig IgG) goat antibody (AP108S, Chemicon).

For triple-immunofluorescence staining for VGluT1, VGluT2, and tyrosine hydroxylase (TH), we treated P0 mouse sections with Mouse on Mouse Kits (M.O.M., Vector) according to the manufacturer's instructions to reduce background caused by endogenous mouse IgG-like molecules. The sections were then incubated overnight with a mixture of 5 μg/ml anti-VGluT1 guinea pig IgG, 5 μg/ml anti-VGluT2 rabbit IgG, and 1:500 diluted anti-TH mouse monoclonal antibody (MAB318, Chemicon), for 1 hour with 1:250 diluted biotinylated anti-(mouse IgG) donkey antibody (Vector) and then finally for 1 hour with 50 μg/ml Cy5-conjugated anti-(guinea pig IgG) antibody, 50 μg/ml Cy3-conjugated anti-(rabbit IgG) antibody (AP182C, Chemicon), and 10 μg/ml AlexaFluor 488-conjugated streptavidin. All the incubation was done at room temperature in PBS-XCD, followed by two washes with PBS-X.

The sections were mounted on APS-coated glass slides and coverslipped with 90% (v/v) glycerol, 2.5% (w/v) triethylenediamine (an antifading reagent), and 20 mM Tris-HCl, pH 7.2. Digital pseudocolor images were captured by a confocal laser-scanning microscope, LSM5 PASCAL (Carl Zeiss, Oberkochen, Germany) with optical slice thickness of less than 1.0 μm, using a 63× water-immersion objective lens (C-Apochromat, NA = 1.2, Carl Zeiss), unless otherwise stated. AlexaFluor 488, Cy3, and Cy5 were excited with 488-, 543-, and 633-nm laser beams and observed through 510–530-, 560–615-, and ≥650-nm emission filters, respectively. When one of the primary antibodies was omitted or replaced with normal IgG for control experiments, no immunofluorescence for the omitted or replaced antibody was detected.

## RESULTS

### Evaluation of immunoreactivity and heat treatment for enhancement of immunoreactivity

The intensity of VGluT immunoreactivity in the immunoperoxidase method was evaluated by using internal standards. VGluT1 immunoreactivity in the medial septal nucleus, caudate-putamen, and layer I of the piriform cortex of P22 mice was used as the internal standards of weak (+), moderate (++), and intense (+++) immunoreactivity (Fig. 1c,g–i), respectively. VGluT2 immunoreactivity of P22 mice was judged to be weak (+) in the stratum lacunosum-moleculare of the hippocampal CA1 region, moderate (++) in the caudate-putamen, and intense (+++) in the medial habenular nucleus (Fig. 1f,j–l). For comparison of the relative intensity between different postnatal ages, the mouse brain sections of each age were processed for immunoperoxidase staining together with a few P22 mouse sections containing these regions for internal standards. For instance, in Figure 1a–f, the sections from P0, P7, and P22 mouse brains were immunostained in the same incubation chamber for VGluT1 (Fig. a–c) or VGluT2 (Fig. d–f), showing clear differences in VGluT immunoreactivity between these ages.

In the double- and triple-immunofluorescence experiments, low immunofluorescence signal may lead to underestimation of coexisting immunoreactivities, especially at small structures, such as axon terminals. We thereby adopted the antigen retrieval technique to avoid underestimation of the colocalization of VGluT1 and VGluT2 immunoreactivities. Of several methods for antigen retrieval, the heat treatment reported by Jiao et al. (1999) was clearly effective in the enhancement of VGluT1 and VGluT2 immunoreactivities (Fig. 1m–p).

### Postnatal changes of VGluT1 and VGluT2 immunoreactivities in mouse forebrain

The postnatal development of VGluT1 and VGluT2 immunoreactivities in the mouse forebrain is summarized in Tables 1 and 2, and Figure 2. At P0, VGluT1 immunoreactivity was intense in most regions of the limbic systems, whereas VGluT2 immunoreactivity was more widely distributed and weak to moderate in the diencephalic regions. During postnatal development, VGluT1 immunoreactivity increased drastically in the neostriatal, neocortical, and diencephalic regions and, at P22, showed similar intensity and distribution to the adult brain. In contrast, VGluT2 immunoreactivity exhibited a less dramatic increase and almost reached the adult level at P14–P22.

Throughout postnatal development, immunoreactivities for both VGluT1 and VGluT2 were predominantly observed in the neuropil of the telencephalic and diencephalic regions (Figs. 1g–l, 2, 5d–f,j–l) and was considered to be located in axon terminals. However, some neuronal cell bodies immu-

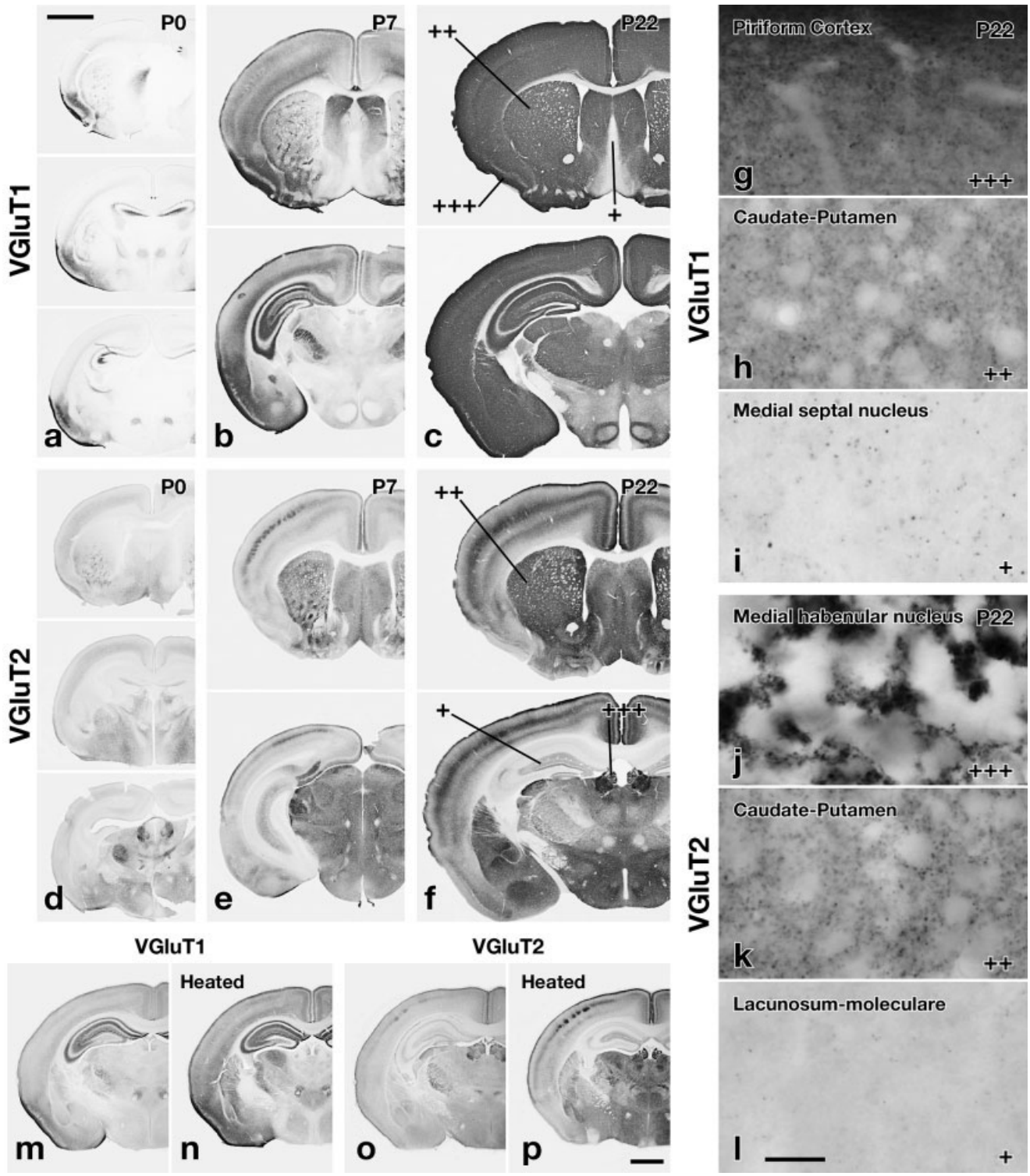


Fig. 1. **a–l:** Comparison of immunoreactivities for VGluT1 and VGluT2 between different postnatal ages. Representative sections from P0 (a,d), P7 (b,e), and P22 (c,f) mice were processed together in the same solution for immunohistochemistry of VGluT1 (a–c) or VGluT2 (d–f). Thus, difference in immunoreactivity can be attributed to the amount of antigen sites in tissue sections. For internal standards, VGluT1 immunoreactivity in P22 brain was defined to be weak (+) in the medial septal nucleus, moderate (++) in the caudate-putamen, and intense (+++) in layer I of the piriform cortex (c,g–i). VGluT2 immunoreactivity in the stratum lacunosum-moleculare of the hippocampal CA1 region, caudate-putamen, and medial habenular nucleus at P22 was defined to be weak (+), moderate (++), and intense (+++), respectively (f,j–l). **m–p:** Effect of antigen retrieval on VGluT1 and VGluT2 immunohistochemistry. Prior to primary antibody incubation, P7 mouse sections were treated by heating at 80°C for 1 hour in 10 mM sodium citrate buffer, pH 6.0. The treated sections showed clearly stronger immunoreactivity (n,p) than untreated ones (m,o). For abbreviations, see list. Scale bars = 1 mm in a (applies to a–f), p (applies to m–p); 20 μm in l (applies to g–l).

TABLE 1. Distribution of Neuropil Immunoreactivity for VGluT1 in the Mouse Forebrain during Postnatal Development[1]

| Region | Neuropil immunoreactivity for VGluT1 | | | | | | | |
|---|---|---|---|---|---|---|---|---|
| | P0 | P1 | P3 | P5 | P7 | P10 | P14 | P22 |
| Olfactory regions | | | | | | | | |
| Main olfactory bulb | | | | | | | | |
| Glomerular layer | +++ | +++ | +++ | +++ | +++ | +++ | ++ | ++ |
| External plexiform layer | +++ | +++ | +++ | +++ | +++ | +++ | +++ | +++ |
| Internal plexiform layer | +++ | +++ | +++ | +++ | +++ | ++ | ++ | ++ |
| Granule cell layer | +++ | +++ | +++ | +++ | +++ | ++ | ++ | ++ |
| Accessory olfactory bulb | ± | ± | + | +~++ | +~++ | ++~+++ | ++~+++ | ++~+++ |
| Olfactory tubercle | ++~+++ | ++~+++ | ++~+++ | ++~+++ | ++~+++ | ++~+++ | ++~+++ | ++~+++ |
| Cerebral cortex | | | | | | | | |
| Neocortex | | | | | | | | |
| Layer I (marginal zone) | ±~+[2] | ±~+[2] | +~++[2] | ++ | ++~+++ | +++ | +++ | +++ |
| Layers II/III | ± | ± | ± | + | + | ++ | ++~+++ | +++ |
| Layer IV | ± | ± | ± | + | +~++ | ++ | ++ | ++ |
| Layer V | ± | ± | ± | + | + | ++ | ++~+++ | ++~+++ |
| Layer VIa | ±~+ | ±~+ | +~++ | ++ | ++ | ++ | ++ | ++ |
| Layer VIb (subplate) | + | + | ++ | ++ | ++ | ++ | ++ | ++ |
| Cingulate cortex | | | | | | | | |
| Layer I | + | + | + | ++ | ++ | ++ | ++~+++ | ++~+++ |
| Layers II–VI | ± | ± | ±~+ | + | + | ++ | ++ | ++ |
| Piriform cortex | | | | | | | | |
| Layer I | +++ | +++ | +++ | +++ | +++ | +++ | +++ | +++ |
| Layer II | ++ | ++ | ++ | ++ | ++ | ++ | ++ | ++ |
| Layer III | ++ | ++~+++ | ++~+++ | ++~+++ | ++~+++ | ++~+++ | +++ | +++ |
| Entorhinal cortex | | | | | | | | |
| Layer I | +++ | +++ | +++ | +++ | +++ | +++ | +++ | +++ |
| Layers II–VI | +~++ | ++ | ++~+++ | ++~+++ | ++~+++ | ++~+++ | ++~+++ | ++~+++ |
| Ammon's horn | | | | | | | | |
| Stratum oriens, CA1 and CA3 | ++ | ++ | +++ | +++ | +++ | +++ | +++ | +++ |
| Stratum oriens, CA2 | ++ | ++ | +++ | +++ | +++ | +++ | +++ | +++ |
| Stratum pyramidale, CA1 and CA3 | − | − | − | − | − | − | − | − |
| Stratum pyramidale, CA2 | − | − | ± | ± | ± | ± | ± | ± |
| Stratum lucidum, CA3 | − | − | − | +++ | +++ | +++ | +++ | +++ |
| Stratum radiatum, CA1–CA3 | ++~+++ | ++~+++ | +++ | +++ | +++ | +++ | +++ | +++ |
| Stratum lacunosum-moleculare, CA1 | ++~+++ | ++~+++ | ++~+++ | ++ | ++ | ++ | ++ | ++ |
| Stratum lacunosum-moleculare, CA2–CA3 | ++~+++ | ++~+++ | +++ | +++ | +++ | +++ | +++ | +++ |
| Dentate gyrus | | | | | | | | |
| Molecular layer | − | ± | +~+++ | ++~+++ | +++ | +++ | +++ | +++ |
| Granular layer | − | − | − | − | − | − | − | − |
| Polymorphic layer | − | − | + | + | ++ | ++ | ++ | +++ |
| Subiculum | + | + | + | +~++ | ++ | ++ | ++~+++ | +++ |
| Septal and basal forebrain regions | | | | | | | | |
| Medial septal nucleus | ± | ± | ± | ± | ± | + | + | + |
| Lateral septal nucleus | ++ | ++ | ++~+++ | ++~+++ | ++~+++ | ++~+++ | ++~+++ | ++~+++ |
| Nucleus of the diagonal band | ± | ± | ± | ± | ± | + | + | + |
| Amygdaloid complex | | | | | | | | |
| Corticomedial amygdaloid nuclear group | +~+++ | ±~+++ | +~+++ | +~+++ | ++~+++ | ++~+++ | ++~+++ | ++~+++ |
| Basolateral amygdaloid nuclear group | ±~+ | ±~+ | +~++ | +~++ | +~++ | ++ | ++ | ++ |
| Basal ganglia, ventral thalamus, and associated nuclei | | | | | | | | |
| Caudate-putamen | | | | | | | | |
| Patches | ++~+++ | ++~+++ | ++~+++ | ++~+++ | ++~+++ | ++ | ++ | ++ |
| Matrix | ± | ± | ±~+ | + | +~++ | ++ | ++ | ++ |
| Accumbens nucleus | ± | + | ±~++ | +~++ | +~++ | ++ | ++ | ++ |
| Globus pallidus | | | | | | | | |
| External segment | ± | ± | ± | ± | ± | ± | ± | ± |
| Internal segment | + | ±~+ | ±~+ | ± | ± | ± | ± | ± |
| Subthalamic nucleus | ± | ± | ± | + | +~++ | +~++ | +~++ | +~++ |
| Epithalamus | | | | | | | | |
| Medial habenular nucleus | ± | + | + | + | +~++ | ++ | ++ | ++ |
| Lateral habenular nucleus | ± | ± | ± | ± | ± | ± | ± | + |
| Dorsal and ventral thalamus | | | | | | | | |
| Anterodorsal and anteroventral nuclei | − | − | ± | ±~+ | + | +~++ | ++ | ++ |
| Anteromedial nucleus | − | − | ± | ±~+ | + | +~++ | ++ | ++ |
| Mediodorsal nucleus | − | − | ± | ± | ±~+ | + | +~++ | ++ |
| Laterodorsal nucleus | − | − | + | +~++ | +~++ | ++ | ++ | ++ |
| Lateroposterior nucleus | − | − | + | +~++ | +~++ | ++ | ++ | ++ |
| Ventroanterior nucleus | − | − | ± | ±~+ | ±~+ | +~++ | +~++ | +~++ |
| Ventrolateral nucleus | − | − | + | + | + | +~++ | +~++ | +~++ |
| Ventral posterolateral nucleus | − | − | − | + | + | ++ | ++~+++ | ++~+++ |
| Ventral posteromedial nucleus | +~++ | +~++ | ++~+++ | ++~+++ | ++~+++ | ++~+++ | ++~+++ | ++~+++ |
| Posterior nuclei | − | ± | + | + | +~++ | ++ | ++~+++ | ++~+++ |
| Intralaminar nuclei | − | − | ± | ± | ±~+ | +~++ | +~++ | +~++ |
| Midline nuclei | − | ± | ± | ± | ±~+ | +~++ | +~++ | +~++ |
| Thalamic reticular nucleus | +~++ | +~++ | ++ | ++ | ++ | ++ | ++ | ++ |
| Dorsal lateral geniculate nucleus | − | − | ± | + | + | +~++ | +~++ | ++ |
| Medial geniculate nucleus | − | − | ± | ±~+ | + | +~++ | +~++ | +~++ |
| Preoptic region and hypothalamus | | | | | | | | |
| Lateral preoptic area | ± | ± | ± | ± | ±~+ | + | + | + |
| Medial preoptic area | ± | ± | ± | ± | ±~+ | + | + | + |
| Anterior hypothalamic area | ± | ± | ± | ± | ±~+ | + | + | + |
| Suprachiasmatic nucleus | − | ± | ± | ± | ± | ± | ± | ± |
| Paraventricular hypothalamic nucleus | +~++ | +~++ | +~++ | ± | ± | ± | ± | + |
| Dorsal hypothalamic area | ± | ± | ± | ± | ±~+ | ±~+ | + | + |
| Lateral hypothalamic area | ± | ± | ± | ± | ± | ±~+ | + | + |
| Periventricular nucleus | ± | ± | ± | ± | ± | ±~+ | + | + |
| Ventromedial hypothalamic nucleus | − | − | ± | + | + | +~++ | +~++ | +~++ |
| Dorsomedial hypothalamic nucleus | + | + | ±~+ | ±~+ | ±~+ | ±~+ | + | + |
| Arcuate nucleus | ± | ± | ± | ± | ± | ± | ± | ± |
| Posterior hypothalamic area | ± | ± | ± | ± | ±~+ | ±~+ | + | + |
| Supramammillary nucleus | ± | ± | ± | ± | ± | + | + | + |
| Mammillary nuclei | ± | ± | ±~+ | ++ | ++ | ++ | ++ | ++ |

[1]Intensity of VGluT1 immunoreactivity at P22 was evaluated using internal standards as follows: layer I of the piriform cortex (+++), caudate-putamen (++), and medial septal nucleus (+). ±, very weak or almost negative; −, negative. Comparison and evaluation of VGluT1 immunoreactivity in other developmental stages was carried out by using internal standards. P22 mouse sections containing the regions for internal standards were processed in the same incubation chamber together with specimens from different postnatal ages.
[2]VGluT1 immunoreactivity in the marginal zone (layer I) of the neocortex was weaker in the lateral neocortical regions than that in the medial neocortical regions from P0 to P3.

TABLE 2. Distribution of Neuropil Immunoreactivity for VGluT2 in the Mouse Forebrain during Postnatal Development[1]

| Region | Neuropil immunoreactivity for VGluT2 | | | | | | | |
|---|---|---|---|---|---|---|---|---|
| | P0 | P1 | P3 | P5 | P7 | P10 | P14 | P22 |
| Olfactory regions | | | | | | | | |
| Main olfactory bulb | | | | | | | | |
| Glomerular layer | +++ | +++ | +++ | +++ | +++ | +++ | +++ | +++ |
| External plexiform layer | ± | ± | ± | ± | ± | ± | ± | ± |
| Internal plexiform layer | + | + | + | + | + | + | + | + |
| Granule cell layer | ± | ± | ± | ± | ± | ± | ± | ± |
| Accessory olfactory bulb | +~++ | +~++ | +~++ | +~++ | +~++ | +~++ | +~++ | +~++ |
| Olfactory tubercle | ±~+ | +~++ | +~++ | +~++ | +~++ | +~++ | +~++ | +~++ |
| Cerebral cortex | | | | | | | | |
| Neocortex | | | | | | | | |
| Layer I (marginal zone) | + | +~++ | ++ | ++~+++ | ++~+++ | +++ | +++ | +++ |
| Layers II/III | ± | ± | ±~+ | + | + | +~++ | +~++ | +~++ |
| Layer IV | ±~+ | +~++ | +~++ | ++ | ++ | ++~+++ | ++~+++ | ++~+++ |
| Layer V | ±~+ | + | + | + | + | + | + | + |
| Layer VIa | + | + | + | + | + | +~++ | +~++ | +~++ |
| Layer VIb (subplate) | + | + | + | + | + | + | + | + |
| Cingulate cortex | | | | | | | | |
| Layer I | + | +~++ | +~++ | ++ | ++ | ++ | ++~+++ | ++~+++ |
| Layers II–VI | ±~+ | ±~+ | + | + | + | +~++ | +~++ | +~++ |
| Piriform cortex | | | | | | | | |
| Layer I | ++ | ++ | ++ | +~++ | + | + | + | + |
| Layer II | ± | ± | ± | + | + | + | + | + |
| Layer III | + | + | + | + | + | + | + | +~++ |
| Entorhinal cortex | | | | | | | | |
| Layer I | ++ | ++ | +~++ | + | + | + | + | + |
| Layers II–VI | + | + | + | + | + | ±~+ | ±~+ | ±~+ |
| Ammon's horn | | | | | | | | |
| Stratum oriens, CA1 and CA3 | ± | ± | ± | ± | ± | ± | ± | ± |
| Stratum oriens, CA2 | ± | ± | ± | ± | ± | ± | + | + |
| Stratum pyramidale, CA1 and CA3 | − | − | − | ± | ± | ± | ± | ± |
| Stratum pyramidale, CA2 | ± | ± | ±~+ | + | + | ++ | ++ | ++ |
| Stratum lucidum, CA3 | − | − | − | ± | ±~+ | ± | ± | − |
| Stratum radiatum, CA1–CA3 | − | − | ± | ± | ± | ± | ± | ± |
| Stratum lacunosum-moleculare, CA1 | + | + | + | + | + | + | + | + |
| Stratum lacunosum-moleculare, CA2–CA3 | + | + | + | + | + | + | + | + |
| Dentate gyrus | | | | | | | | |
| Molecular layer | + | + | + | + | + | + | + | + |
| Granular layer | − | − | − | + | + | ++ | ++ | ++ |
| Polymorphic layer | − | − | − | ± | ± | ± | ± | − |
| Subiculum | − | − | ± | + | + | + | +~++ | +~++ |
| Septal and basal forebrain regions | | | | | | | | |
| Medial septal nucleus | + | + | +~++ | +~++ | +~++ | +~++ | ++ | ++ |
| Lateral septal nucleus | + | + | +~++ | +~++ | +~++ | +~++ | +~++ | +~++ |
| Nucleus of the diagonal band | + | + | +~++ | ++ | ++ | ++ | ++ | ++ |
| Amygdaloid complex | | | | | | | | |
| Corticomedial amygdaloid nuclear group | +~+++ | +~+++ | +~+++ | +~+++ | +~+++ | +~+++ | +~+++ | +~+++ |
| Basolateral amygdaloid nuclear group | ±~+ | ±~+ | +~++ | +~++ | +~++ | ++ | ++ | ++ |
| Basal ganglia, ventral thalamus, and associated nuclei | | | | | | | | |
| Caudate-putamen | | | | | | | | |
| Patches | +++ | +++ | +++ | +++ | +++ | ++~+++ | ++ | ++ |
| Matrix | + | + | +~++ | +~++ | +~++ | ++ | ++ | ++ |
| Accumbens nucleus | − | ± | ±~++ | +~++ | ++~+++ | ++~+++ | ++~+++ | ++~+++ |
| Globus pallidus | | | | | | | | |
| External segment | ++ | ++ | ++ | +~++ | +~++ | +~++ | +~++ | +~++ |
| Internal segment | ++ | ++ | ++ | +~++ | +~++ | +~++ | +~++ | +~++ |
| Subthalamic nucleus | ±~+ | + | + | +~++ | +~++ | ++ | ++ | ++ |
| Epithalamus | | | | | | | | |
| Medial habenular nucleus | ++ | ++ | +++ | +++ | +++ | +++ | +++ | +++ |
| Lateral habenular nucleus | ++~+++ | ++~+++ | +++ | +++ | +++ | +++ | +++ | +++ |
| Dorsal and ventral thalamus | | | | | | | | |
| Anterodorsal and anteroventral nuclei | ± | + | ++ | ++~+++ | +++ | +++ | +++ | +++ |
| Anteromedial nucleus | +~++ | +~++ | ++~+++ | ++~+++ | ++~+++ | ++~+++ | ++~+++ | ++~+++ |
| Mediodorsal nucleus | + | + | +~++ | +~++ | ++ | +~++ | +~++ | +~++ |
| Laterodorsal nucleus | + | + | +~++ | ++ | ++ | ++ | ++ | ++ |
| Lateroposterior nucleus | + | + | +~++ | ++ | ++ | ++ | ++ | ++ |
| Ventroanterior nucleus | ± | ± | + | + | + | + | + | + |
| Ventrolateral nucleus | + | + | +~++ | ++ | ++ | ++ | ++ | ++ |
| Ventral posterolateral nucleus | ++ | ++ | ++~+++ | +++ | +++ | ++~+++ | ++ | +~++ |
| Ventral posteromedial nucleus | ++ | ++ | ++~+++ | +++ | +++ | ++~+++ | ++ | +~++ |
| Posterior nuclei | + | + | +~++ | ++ | ++ | ++ | +~++ | + |
| Intralaminar nuclei | +~++ | +~++ | +~++ | ++ | ++ | ++ | ++ | ++ |
| Midline nuclei | ±~+ | + | +~++ | ++ | ++ | ++ | ++ | ++ |
| Thalamic reticular nucleus | + | + | +~++ | ++ | ++ | ++ | ++ | ++ |
| Dorsal lateral geniculate nucleus | ±~+ | + | +~++ | ++~+++ | +++ | +++ | +++ | +++ |
| Medial geniculate nucleus | ++ | ++ | ++ | ++~+++ | ++~+++ | ++~+++ | ++~+++ | ++~+++ |
| Preoptic region and hypothalamus | | | | | | | | |
| Lateral preoptic area | ++ | ++ | ++ | ++ | ++ | ++ | ++~+++ | ++~+++ |
| Medial preoptic area | + | + | +~++ | ++ | ++ | ++ | ++~+++ | ++~+++ |
| Anterior hypothalamic area | + | + | +~++ | ++ | ++ | ++ | ++~+++ | ++~+++ |
| Suprachiasmatic nucleus | ± | ± | ± | + | + | + | +~++ | ++ |
| Paraventricular hypothalamic nucleus | ++ | ++ | ++ | ++ | ++ | ++ | ++~+++ | ++~+++ |
| Dorsal hypothalamic area | +~++ | +~++ | +~++ | ++ | ++ | ++ | ++~+++ | ++~+++ |
| Lateral hypothalamic area | +~++ | +~++ | +~++ | ++ | ++ | ++ | ++~+++ | ++~+++ |
| Periventricular nucleus | + | + | +~++ | ++ | ++ | ++ | ++~+++ | ++~+++ |
| Ventromedial hypothalamic nucleus | +~++ | +~++ | ++ | ++~+++ | ++~+++ | ++~+++ | +++ | +++ |
| Dorsomedial hypothalamic nucleus | + | + | +~++ | ++ | ++ | ++ | ++~+++ | ++~+++ |
| Arcuate nucleus | ± | + | +~++ | ++ | ++ | ++ | ++~+++ | ++~+++ |
| Posterior hypothalamic area | + | +~++ | +~++ | ++ | ++ | ++ | ++~+++ | ++~+++ |
| Supramammillary nucleus | + | +~++ | +~++ | ++ | ++ | ++ | ++~+++ | ++~+++ |
| Mammillary nuclei | ± | + | +~++ | +~++ | +~++ | +~++ | ++~+++ | ++~+++ |

[1]Intensity of VGluT2 immunoreactivity at P22 was evaluated using internal standards as follows: layer I of the medial habenular nucleus (+++), caudate-putamen (++), and stratum lacunosum-moleculare of CA1 (+). ±, very weak or almost negative; −, negative. Comparison and evaluation of VGluT2 immunoreactivity in other developmental stages was carried out by using internal standards. P22 mouse sections containing the regions for internal standards were processed in the same incubation chamber together with specimens from different postnatal ages.

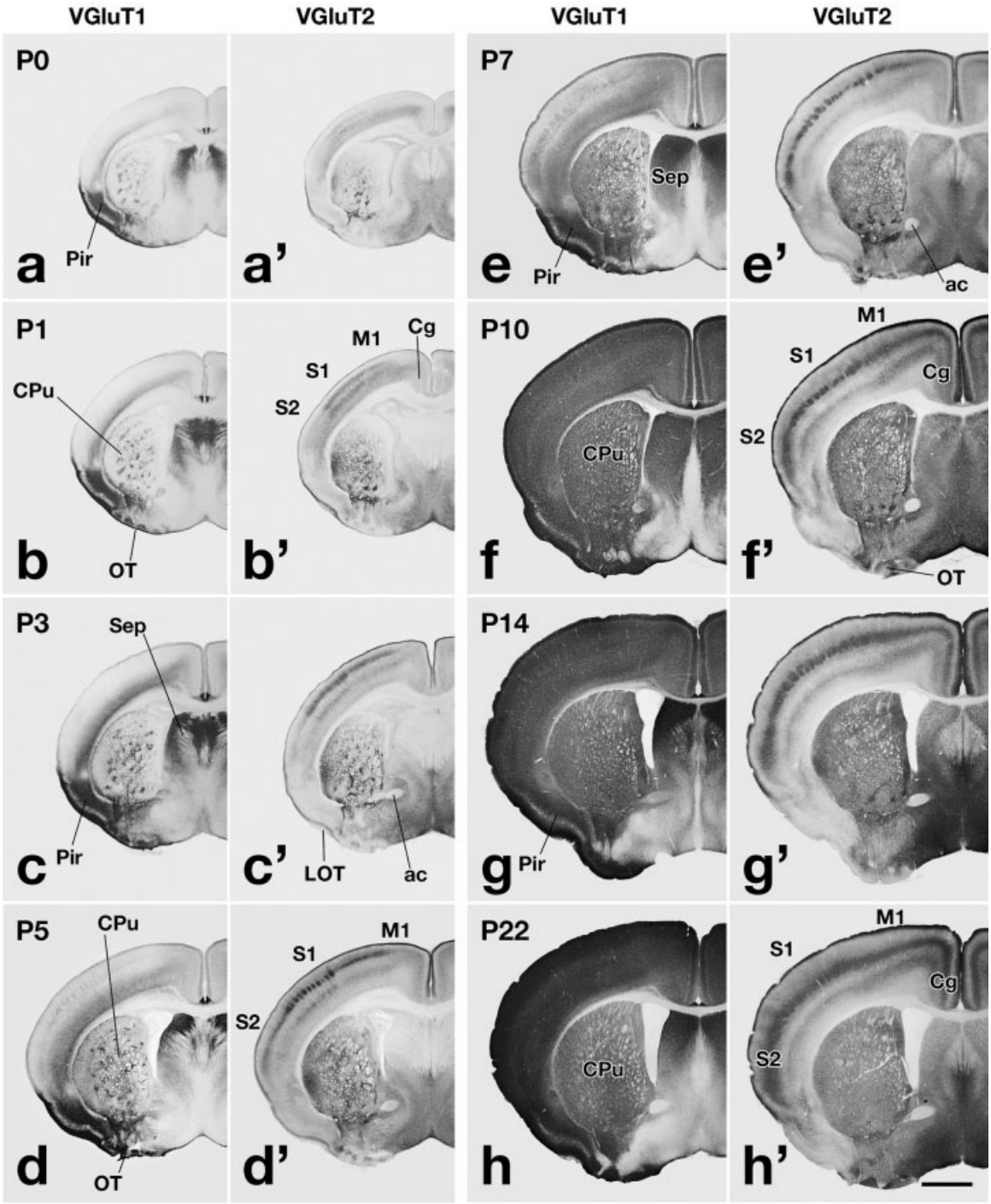


Fig. 2. Immunohistochemical localization of VGluT1 and VGluT2 immunoreactivities in the postnatal developing mouse forebrain. Frontal sections through the caudate-putamen (**a–h′**), thalamic ventrobasal nuclear complex (**i–p′**), and superior colliculus (**q–x′**) at P0–P22 were shown. A letter and a letter with a prime sign indicate consecutive sections immunostained for VGluT1 and VGluT2, respectively. For abbreviations, see list. Scale bars = 1 mm in h′ (applies to a–h′), p′ (applies to i–p′), x′ (applies to q–x′).

noreactive for VGluT1 or VGluT2 were found in the olfactory bulb and piriform cortex from P0 to P7 (Fig. 3g–j,l,n). Putative axon fibers with weak to moderate VGluT1 immunoreactivity were seen in the white matter, such as the fornix, fimbria, and internal capsule before P7 (Figs. 6a,b, 8a–c), and the fasciculus retroflexus throughout postnatal development (Figs. 2q–x, 8d). These findings suggest that during postnatal development some VGluT immunoreactivity was observed at the neuronal portions where the protein was synthesized or transported.

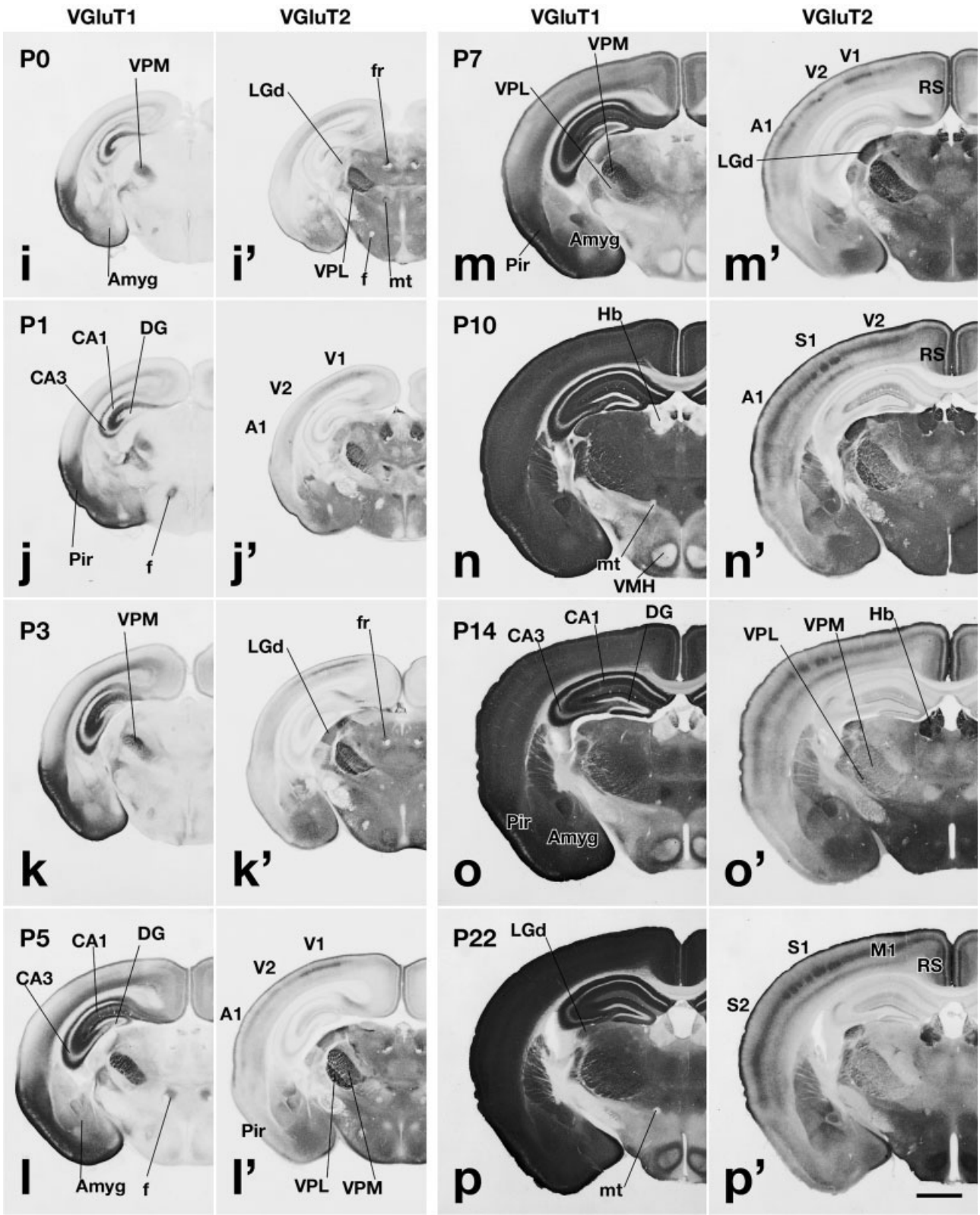


Figure 2 (Continued)

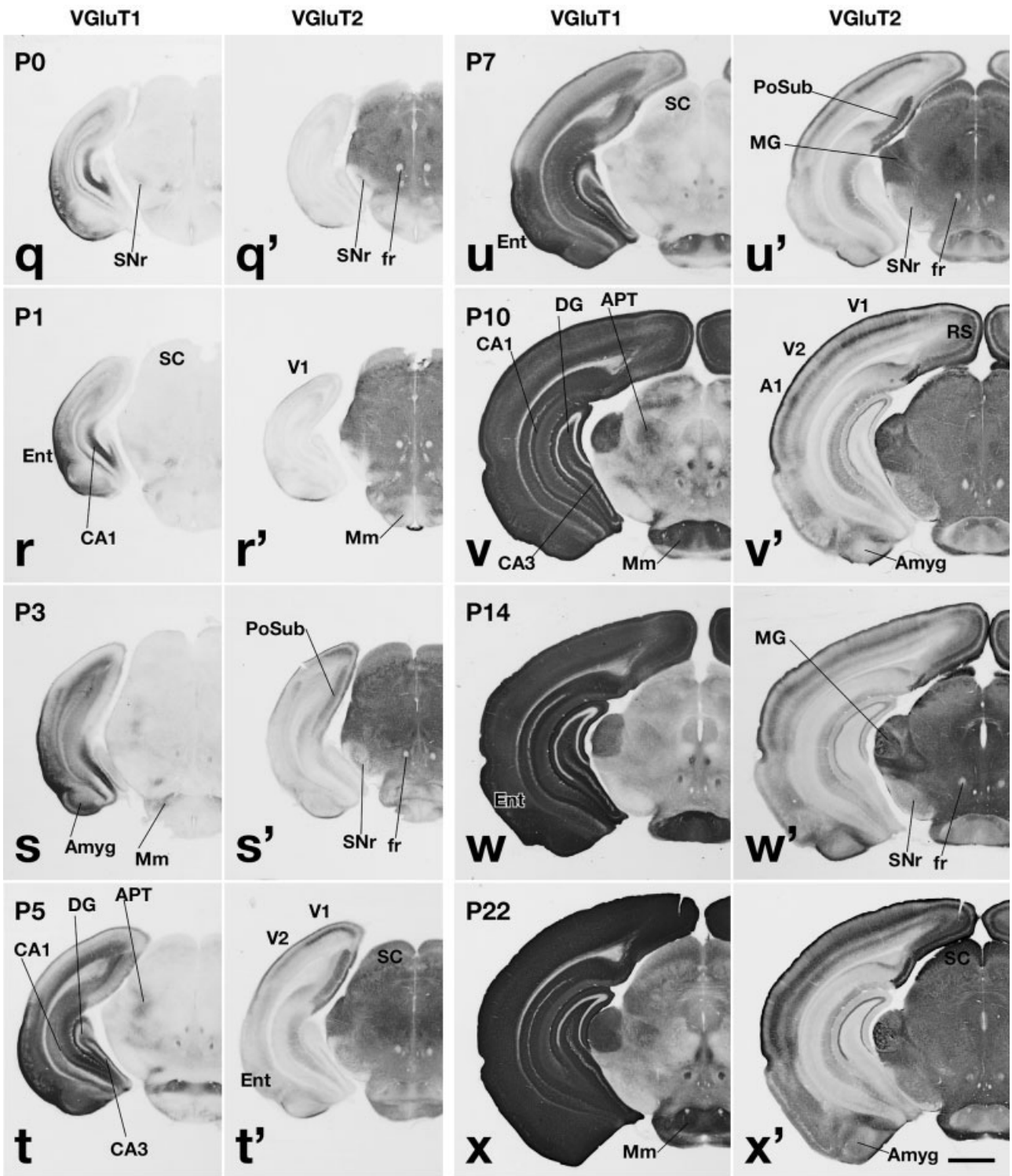


Figure 2 (Continued)

## Olfactory bulb and associated regions

In the main olfactory bulb, VGluT immunoreactivity of each layer showed only slight changes throughout postnatal development (Fig. 3a–f). VGluT1 immunoreactivity was intense in the external plexiform, internal plexiform, and granule cell layers from P0 to adulthood, whereas VGluT2 immunoreactivity was weak or very weak in these

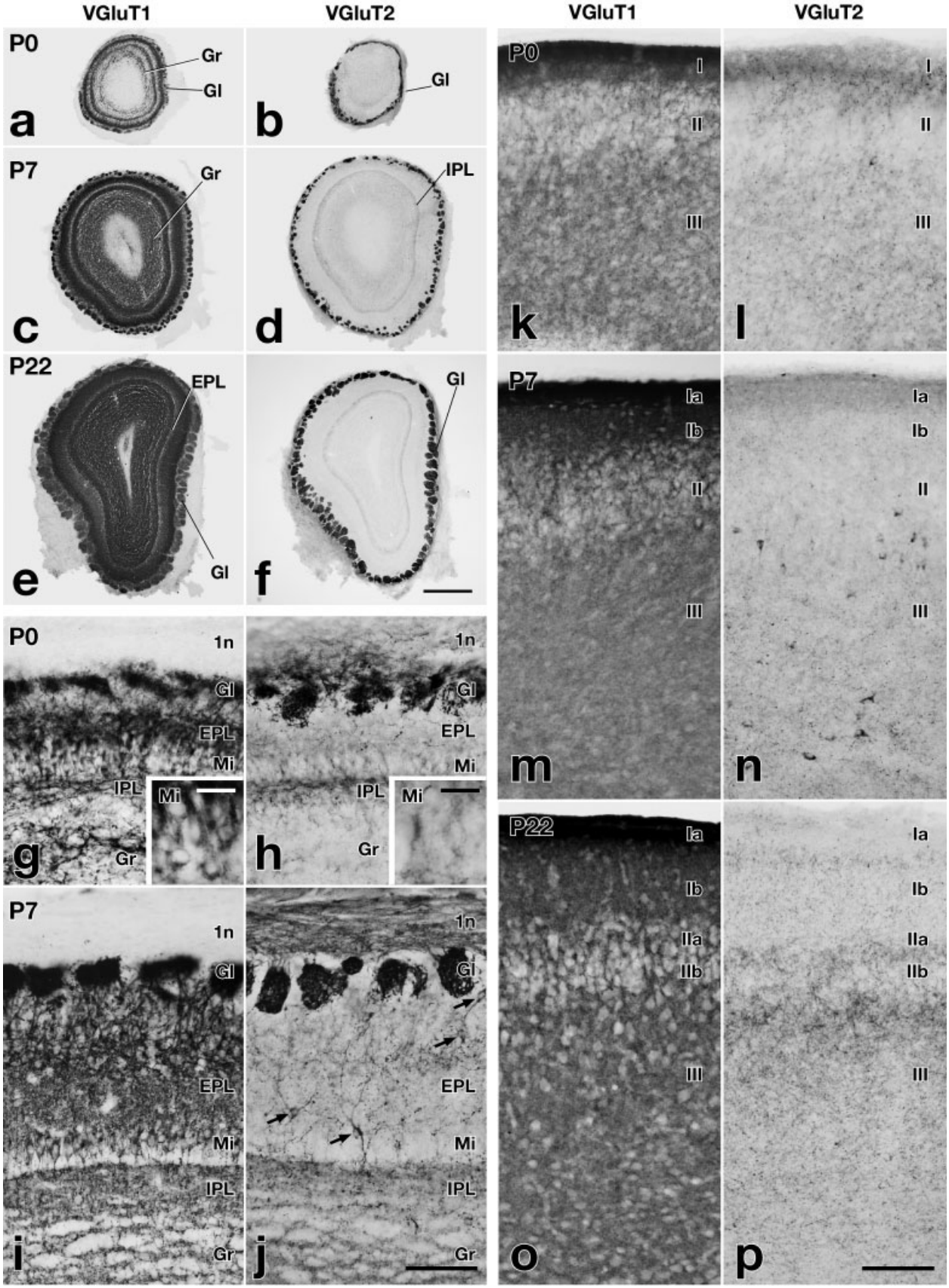


Fig. 3. VGluT1 and VGluT2 immunoreactivities in the postnatal developing olfactory bulb and piriform cortex. **a–f:** VGluT1 and VGluT2 immunoreactivities in the olfactory bulb at P0 (a,b), P7 (c,d), and P22 (e,f). Although the size of the olfactory bulb increased markedly, VGluT1 and VGluT2 immunoreactivities of each layer showed only a few changes from P0 to P22. **g–j:** The olfactory bulb at P0 (g,h) and P7 (i,j) immunostained for VGluT1 and VGluT2 at higher magnification. Note that neuronal cell bodies in the mitral cell layer at P0 were intensely immunoreactive for VGluT1 (inset in g) and very weakly immunoreactive for VGluT2 (inset in h) and that a few scattered neuronal cell bodies in the P7 external plexiform layer were immunoreactive for VGluT2 (arrows in j). **k–p:** VGluT1 and VGluT2 immunoreactivities in the piriform cortex at P0 (k,l), P7 (m,n), and P22 (o,p). Note that moderate immunoreactivity for VGluT2 in layer I was observed at P0, but not at P7 or P22. In contrast, intense VGluT1 immunoreactivity was observed throughout postnatal development. For abbreviations, see list. Scale bars = 500 μm in f (applies to a–f); 100 μm in j (applies to a–j), p (applies to k–p); 20 μm in insets g,h.

layers. In the external plexiform layer, a few moderately VGluT2-immunoreactive neuronal cell bodies were observed from P0 to P22, which increased slightly in number after P5 (arrows, Fig. 3j). These cells might be tufted cells, as they were located in the external plexiform layer, and their dendrites extended toward glomeruli. In the mitral cell layer, many neuronal cell bodies showed intense VGluT1 immunoreactivity from P0 to P7 (inset, Fig. 3g) and became less immunoreactive in later postnatal stages. Very weak or faint VGluT2 immunoreactivity was observed in numerous neuronal cell bodies in the mitral cell layer from P0 to P3 (inset, Fig. 3h) but disappeared by P5. In the glomerular layer or at the boundary of the external plexiform layer and glomerular layer, VGluT1-immunoreactive neuronal cell bodies were observed after P5. Because their dendrites extended into glomeruli, these cells might be considered as external tufted cells or a non-GABAergic subtype of periglomerular cells (Hayar et al., 2004). Glomeruli in the olfactory bulb showed intense VGluT2 immunoreactivity throughout postnatal development, whereas they displayed intense and moderate VGluT1 immunoreactivity before P10 and after P14, respectively (Fig. 3a–j). Double-immunofluorescence staining for VGluT1 and VGluT2 revealed that the vast majority of punctae in the glomeruli were immunoreactive for either VGluT1 or VGluT2 alone from P0 to P22 (Fig. 4a–b′′), suggesting that these two kinds of punctae were different in origin. Because many neuronal cell bodies of the mitral cell layer showed intense VGluT1 immunoreactivity in early postnatal stages, primary dendritic tufts of mitral cells were assumed to be VGluT1-immunoreactive in the glomeruli. At least some of the VGluT2-immunoreactive punctae in the glomeruli may be axon terminals of olfactory sensory neurons, because fibers in the olfactory nerve layer showed weak to moderate VGluT2 immunoreactivity but did not display VGluT1 immunoreactivity throughout postnatal development (Fig. 3g–j).

In the piriform cortex, intense and moderate to intense VGluT1 immunoreactivity was observed in layer I and layer II/III, respectively, throughout postnatal development (Figs. 2a–p, 3k,m,o). Although VGluT2 immunoreactivity in layer II/III showed a little increase and became weak to moderate throughout development, VGluT2 immunoreactivity in the superficial part of layer I (layer Ia) was moderate at P0, rapidly decreased from P5 to P7, and was almost negative after P10 (Figs. 2a′–p′, 3l,n,p). Double-immunofluorescence staining revealed that VGluT1 and VGluT2 immunoreactivities were frequently colocalized in single putative axon terminals in layer Ia of the P0 piriform cortex (Fig. 4c–c′′). Because layer Ia is known to receive exclusively afferent fibers from mitral/tufted cells of the main olfactory bulb (Shepherd, 2004), these observations suggest that mitral/tufted cells may express both the VGluTs in early postnatal period but VGluT1 alone in adulthood. This was in agreement with the finding that VGluT2-immunoreactive cell bodies were observed only at P0–P3 in the mitral cell layer of the main olfactory bulb. In layer III, a few scattered neuronal cell bodies were weakly or moderately immunoreactive for VGluT2 throughout postnatal development (Fig. 3l,n).

In the accessory olfactory bulb, VGluT1 immunoreactivity was very weak at P0 and gradually increased after P3. Glomeruli of the accessory olfactory bulb showed moderate VGluT2 immunoreactivity at P0. In contrast, the glomeruli displayed almost no VGluT1 immunoreactivity at P0, became immunoreactive for VGluT1 after P3, and exhibited moderate to intense VGluT1 immunoreactivity after P10. Thus, VGluT1 immunoreactivity in the accessory bulb emerged later than that in the main bulb, suggesting slower maturation of the circuitry associated with sexual behavior. The olfactory tubercle showed moderate to intense immunoreactivity for VGluT1 and weak to moderate immunoreactivity for VGluT2 throughout postnatal development (Fig. 2a–h′).

## Neocortex

VGluT2 immunoreactivity was weak at P0 and gradually increased in the neocortex during 2 postnatal weeks (Figs. 2a′–x′, 5g–i). In layer I (the marginal zone), VGluT2 immunoreactivity was weak at P0, moderate to intense from P5 to P7, and intense after P10 (Fig. 5g–i). The subplate (layer VIb) and deep part of layer VIa showed weak VGluT2 immunoreactivity throughout postnatal development. In the lower part of the undifferentiated cortical plate and upper part of layer VI, weak to moderate VGluT2 immunoreactivity was observed at P0 in the primary somatosensory area (area S1). In the other neocortical areas, weak to moderate VGluT2 immunoreactivity emerged at P1 in the lower part of the undifferentiated cortical plate and upper part of layer VI. From P1 to P3, layer IV and the upper part of layer VI of area S1 and the primary motor area (area M1) showed moderate VGluT2 immunoreactivity and were distinctly more immunoreactive than the adjacent neocortical areas (Fig. 2a′–c′). Similarly, these two layers of the primary visual area (area V1) displayed moderate VGluT2 immunoreactivity and were more immunoreactive than adjacent areas from P1 to P10 (Fig. 2j′–m′,r′–v′). VGluT2 immunoreactivity of these two layers became moderate to intense and almost equal between neocortical areas after P14 (Fig. 2g′,h′,o′,p′,w′,x′). Barrel-like clustering of moderately to intensely VGluT2-immunoreactive neuropil was indistinct earlier than P3 and became conspicuous after P5 in layer IV of area S1 (Fig. 2a′–h′). Layer II/III showed weaker VGluT2 immunoreactivity than layer IV throughout postnatal development, but the difference was less distinct after P10 (Fig. 5i). Layer V displayed weak VGluT2 immunoreactivity throughout postnatal development.

VGluT1 immunoreactivity showed much more conspicuous changes in the developing neocortex (Figs. 2a–x, 5a–c). In layer I, VGluT1 immunoreactivity was very weak in lateral neocortical areas and weak in medial neocortical areas from P0 to P3. VGluT1 immunoreactivity in layer I showed a progressive increase from P5 to P10 and became intense after P10 (Fig. 5a–c). In layer VIa and the subplate (layer VIb), VGluT1 immunoreactivity was weak at P0 and moderate after P5 (Fig. 5a–c). VGluT1 immunoreactivity in the subplate was slightly stronger than that of layer VIa from P0 to P7. In layers II–V, VGluT1 immunoreactivity was almost negative at P0, weak at P5, showed progressive increase during the second and third postnatal weeks, and became intense at P22 (Fig. 5a–f). Barrel-like clustering of moderately VGluT1-immunoreactive neuropil was observed from P5 to P7 in layer IV of area S1 (Fig. 5b) but later became inconspicuous because VGluT1 immunoreactivity increased in layer II/III and the septal region of layer IV (Fig. 5c).

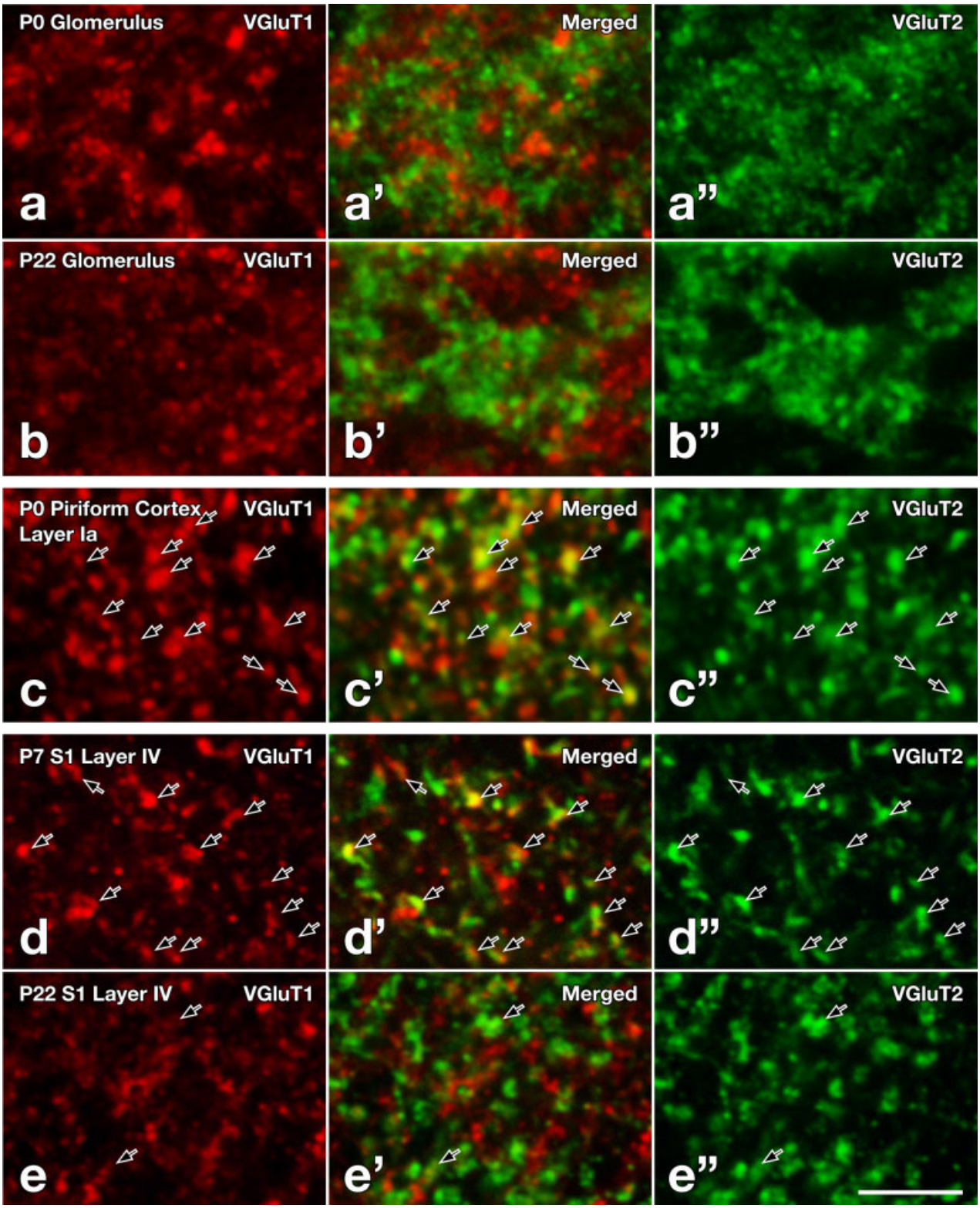


Fig. 4. Confocal laser-scanning microscopic analysis of double-immunofluorescence staining for VGluT1 (red) and VGluT2 (green) in the olfactory bulb, piriform cortex, and barrel hollows in layer IV of the primary somatosensory area (area S1) during postnatal development. **a–b′′:** VGluT1 and VGluT2 immunoreactivities were not colocalized at P0 (a–a′′) and P22 (b–b′′) in olfactory glomeruli. **c–c′′:** VGluT1 and VGluT2 immunoreactivities were frequently colocalized at axon terminal-like profiles (arrows) in layer Ia of P0 piriform cortex. **d–e′′:** In the barrel hollows in layer IV of area S1, VGluT1 immunoreactivity was often colocalized with VGluT2 immunoreactivity in the hollow of the barrel at P7 (arrows in d–d′′), but not at P22 (arrows in e–e′′). Scale bar = 5 μm in e′′ (applies to a–e′′).

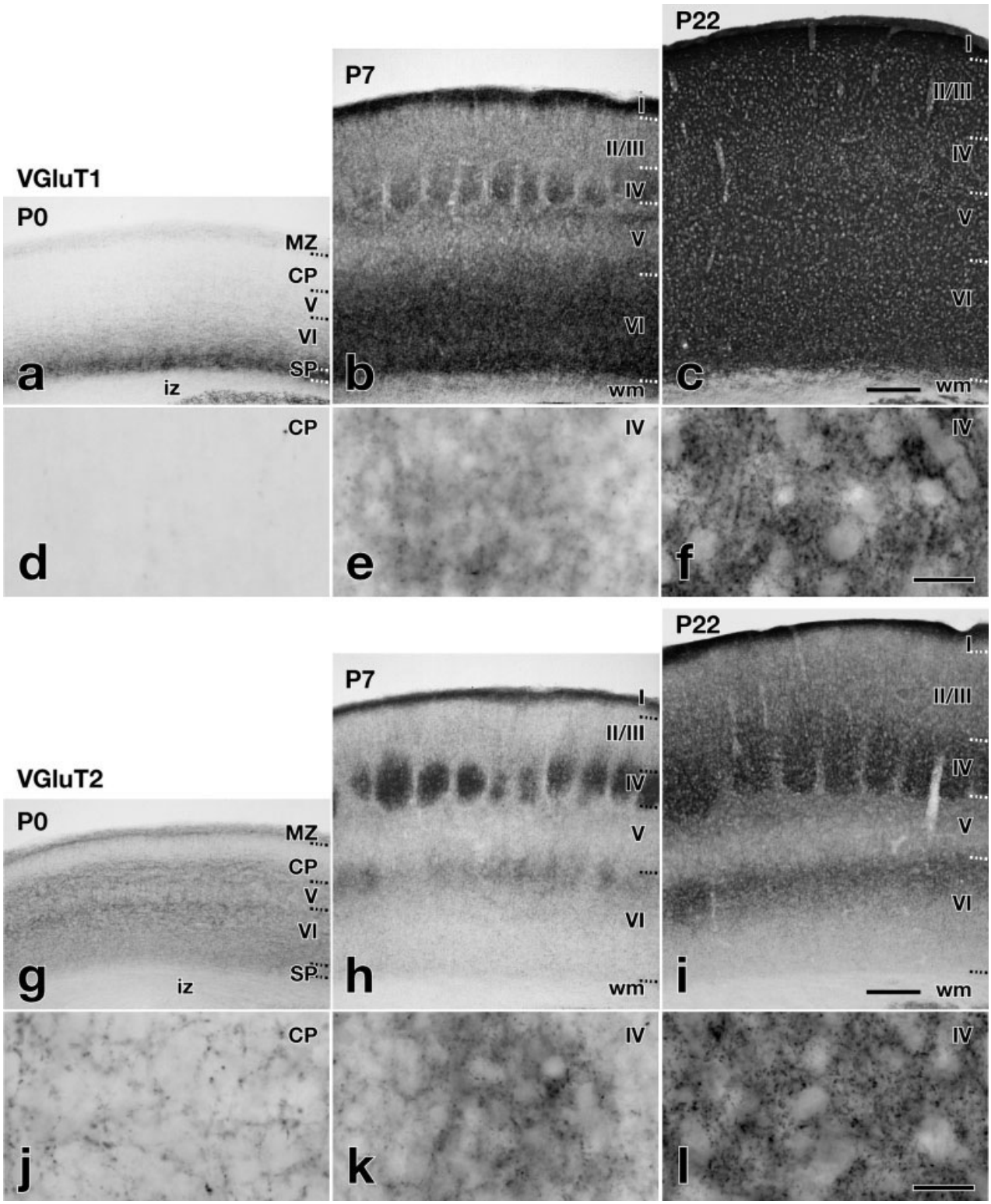


Fig. 5. VGluT1 and VGluT2 immunoreactivities in the postnatal developing primary somatosensory area. VGluT1 and VGluT2 immunoreactivities in the entire cortical thickness at P0 (**a,g**), P7 (**b,h**), and P22 (**c,i**), and in the deep part of undifferentiated cortical plate at P0 (**d,j**), in layer IV at P7 (**e,k**), and in layer IV at P22 (**f,l**) were shown. Note that barrel-like structures were observed in layer IV of the P7 primary somatosensory area of both VGluT1- and VGluT2-immunostained sections (b,h). For abbreviations, see list. Scale bars = 200 μm in c (applies to a–c), i (applies to g–i); 20 μm in f (applies to d–f), l (applies to j–l).

Double-immunofluorescence staining revealed that VGluT1 and VGluT2 immunoreactivities were infrequently colocalized in area S1 at P0. These immunoreactivities were, however, frequently colocalized at single putative axon terminals in the barrel hollows from P5 to P10 (Fig. 4d–d′′), although there were many punctae immunoreactive for VGluT1 or VGluT2 alone. At P22, the frequency of the colocalization greatly decreased in the barrel hollows (Fig. 4e–e′′), indicating that the frequent colocalization of the two VGluTs was a transient event in the barrel hollows of area S1 during postnatal development. In other neocortical areas, such as area M1, area V1, and the forelimb/hindlimb subregion of area S1, colocalization of the immunoreactivities of the two VGluTs was inconspicuous throughout postnatal development.

## Hippocampal formation

VGluT1 immunoreactivity was moderate to intense in neuropil of the stratum oriens, stratum radiatum, and stratum lacunosum-moleculare of Ammon's horn throughout postnatal development (Figs. 2i, 6a–c). In contrast, the stratum pyramidale of Ammon's horn showed almost no VGluT1 immunoreactivity throughout postnatal development (Figs. 2i, 6a). The stratum lucidum of CA3 showed no VGluT1 immunoreactivity until P3 but intense VGluT1 immunoreactivity after P5. Weakly to moderately VGluT1-immunoreactive fibers were observed in the fornix from P0 to P5 (Figs. 2i–l, 8b,c) and in the fimbria from P0 to P7 (Figs. 6a,b, 8a–c,f,g).

VGluT2 immunoreactivity was weak in the stratum lacunosum-moleculare of Ammon's horn from P0 to adulthood (Fig. 6a′–c′). VGluT2 immunoreactivity was negative or very weak in the stratum pyramidale, stratum oriens, and stratum radiatum (Fig. 6a′–c′). In the stratum pyramidale of CA2, weak VGluT2 immunoreactivity appeared around P5 and became moderate by P10. In the stratum lucidum of CA3, very weak VGluT2 immunoreactivity was observed from P5 to P14 but disappeared at P22. VGluT2 immunoreactivity in the stratum lucidum was much weaker in the temporal part than in the septal part of Ammon's horn.

Double-immunofluorescence staining revealed that, in the stratum lucidum of CA3, VGluT1 and VGluT2 immunoreactivities were transiently colocalized from P5 to P14 at single large punctae (~3 μm in diameter; arrows in Fig. 6d–d′′), although smaller (~0.1 μm in diameter) VGluT2 immunoreactivity was not colocalized with VGluT1 immunoreactivity. At P22 and in adulthood, the large punctae were immunoreactive for VGluT1 alone, and the small punctae were immunoreactive for VGluT2 alone (Fig. 6e–e′′). In the stratum lacunosum-moleculare of Ammon's horn, VGluT1 and VGluT2 immunoreactivities were colocalized at a few axon terminal-like punctae throughout postnatal development (arrows in Fig. 6g,j). Almost no colocalization of VGluT1 and VGluT2 immunoreactivities was found at single putative axon terminals in the stratum radiatum (Fig. 6f,i) or stratum oriens of CA1 throughout postnatal development.

The dentate gyrus showed almost no VGluT1 immunoreactivity at P0 (Fig. 6a), and VGluT1 immunoreactivity first appeared at P1 and P3 in the molecular layer and hilar region, respectively. VGluT1 immunoreactivity in the molecular layer increased and became intense by P7, whereas that in the hilar region gradually increased until P22. VGluT2 immunoreactivity in the molecular layer was moderate at P0 (Fig. 6a′). VGluT2 immunoreactivity in the outer part of the granule cell layer appeared at P5 and became moderate by P10 (Fig. 6b′,c′). Very weak VGluT2 immunoreactivity was observed in the hilar region from P5 to P14 but disappeared after P22. Double-immunofluorescence staining revealed that a few axon terminal-like punctae in the molecular layer of the dentate gyrus were immunoreactive for both the VGluTs after P5 (arrows in Fig. 6h,k). In the hilar region, almost all intensely VGluT1-immunoreactive large punctae showed very weak VGluT2 immunoreactivity from P5 to P14, but not at P22. This transient colocalization was very similar to that of the stratum lucidum of CA3.

The entorhinal cortex displayed moderate to intense immunoreactivity for VGluT1 throughout postnatal development (Fig. 2q–x). In contrast, VGluT2 immunoreactivity in layer I was moderate from P0 to P3 and became weak by P5. In layers II–VI, VGluT2 immunoreactivity was weak throughout postnatal development (Fig. 2q′–x′). The early emergence of VGluT1-immunoreactive terminals and the decrease of VGluT2 immunoreactivity in layer I during development were similar to those of the piriform cortex.

## Septum, basal forebrain, and amygdala

The lateral septal nucleus displayed moderate to intense VGluT1 immunoreactivity (Fig. 2a–h), whereas the medial septal nucleus and nucleus of the diagonal band showed faint to weak immunoreactivity for VGluT1 throughout postnatal development. VGluT2 immunoreactivity in the medial and lateral septal nuclei and nucleus of the diagonal band was weak at P0 and became moderate after P5 (Fig. 2a′–h′).

In the amygdaloid complex, most corticomedial nuclei including the amygdalohippocampal area and anterior, central, cortical, and medial amygdaloid nuclei showed weak to intense VGluT1 immunoreactivity at P0. In contrast, very weak immunoreactivity for VGluT1 was observed at P0 in the basolateral nuclei, which were composed of the basolateral, basomedial, and lateral amygdaloid nuclei (Fig. 2i). In both regions, VGluT1 immunoreactivity gradually increased until P10 and became moderate to intense (Fig. 2i–p). VGluT2 immunoreactivity in the corticomedial nuclei was weak to intense and did not show marked changes during postnatal development, whereas that in the basolateral nuclei was weak at P0 and became moderate after P10 (Fig. 2i′–p′). These results suggest that glutamatergic axon terminals mature earlier in the corticomedial nuclei, which are known to receive inputs directly through the lateral olfactory tract, than in the basolateral nuclei.

## Basal ganglia and associated regions

Patchy regions in the caudate-putamen showed moderate to intense immunoreactivities for both VGluT1 and VGluT2 from P0 to P7 (Fig. 2a–e,a′–e′). The striatal patches (striosomes or dopamine islands) are known to show higher TH immunoreactivity than the matrix at birth (Graybiel et al., 1981; for review, see Gerfen, 1992). We hence performed triple-immunofluorescence staining for TH and the two VGluTs using P0 mouse sections. The striatal patches, showing intense TH immunoreactivity, were moderately to intensely immunoreactive for both VGluT1 and VGluT2 (arrows, Fig. 7a–a′′). In the matrix of P0 striatum, VGluT1 immunoreactivity was very weak,

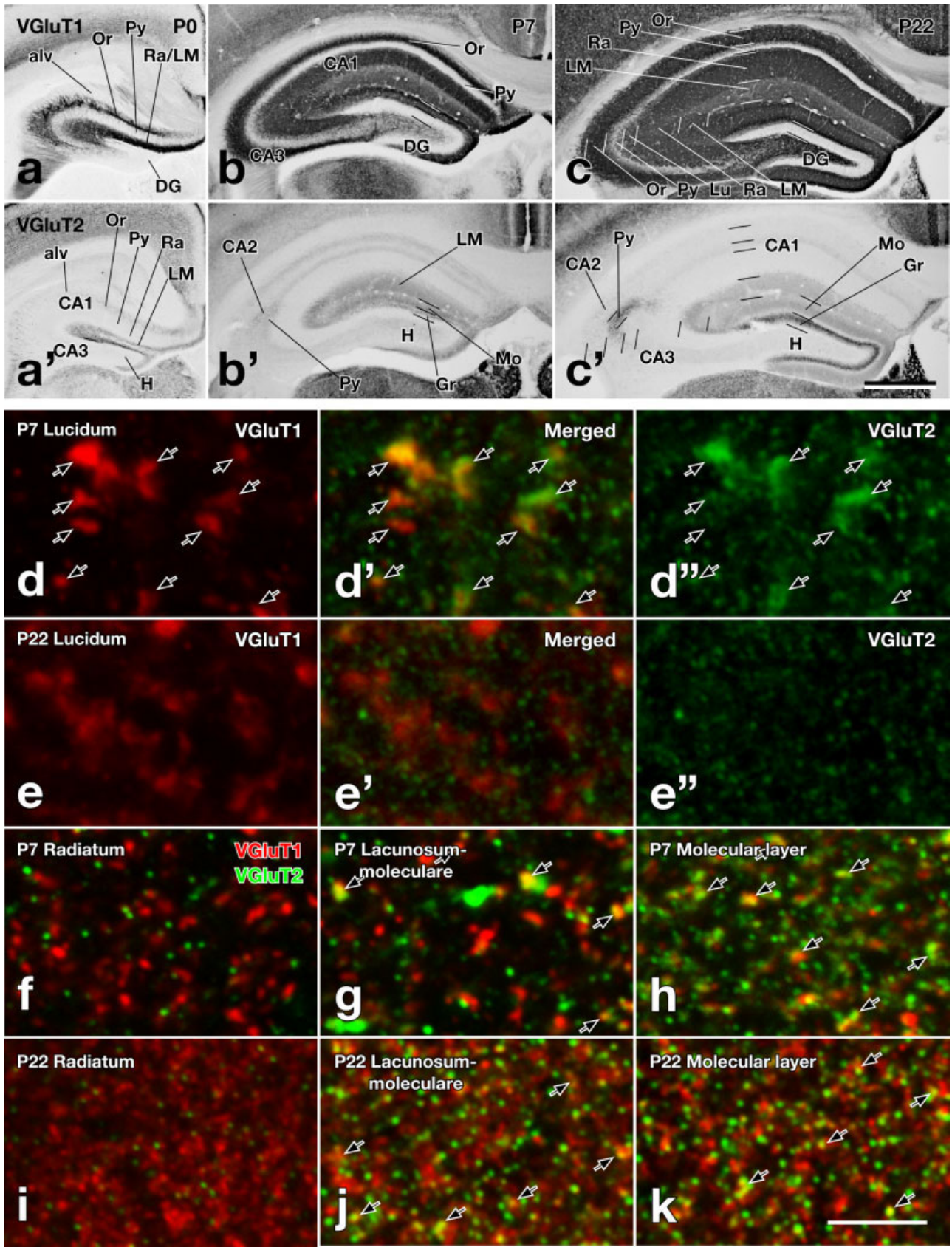


Fig. 6. VGluT1 and VGluT2 immunoreactivities in the postnatal developing hippocampus. **a–c′:** VGluT1 and VGluT2 immunoreactivities in the hippocampal formation at P0 (a,a′), P7 (b,b′), and P22 (c,c′). A letter and a letter with a prime sign indicate consecutive sections immunostained for VGluT1 and VGluT2, respectively. **d–k:** Confocal laser-scanning microscopic images of double-immunofluorescence staining for VGluT1 (red) and VGluT2 (green) in the stratum lucidum of CA3 at P7 (d–d′′) and P22 (e–e′′), the stratum radiatum of CA1 at P7 (f) and P22 (i), the stratum lacunosum-moleculare of CA1 at P7 (g) and P22 (j), and the molecular layer of the dentate gyrus at P7 (h) and P22 (k). Note that most large punctae immunoreactive for VGluT1 showed VGluT2 immunoreactivity at P7 (arrows in d–d′′) but not at P22 (e–e′′) in the stratum lucidum of CA3. Some VGluT1 immunoreactivity was colocalized with VGluT2 immunoreactivity in the stratum lacunosum-moleculare of CA1 (arrows in g,j) and the molecular layer of the dentate gyrus (arrows in h,k), both at P7 and P22. For abbreviations, see list. Scale bars = 500 μm in c′ (applies to a–c′); 5 μm in k (applies to d–k).

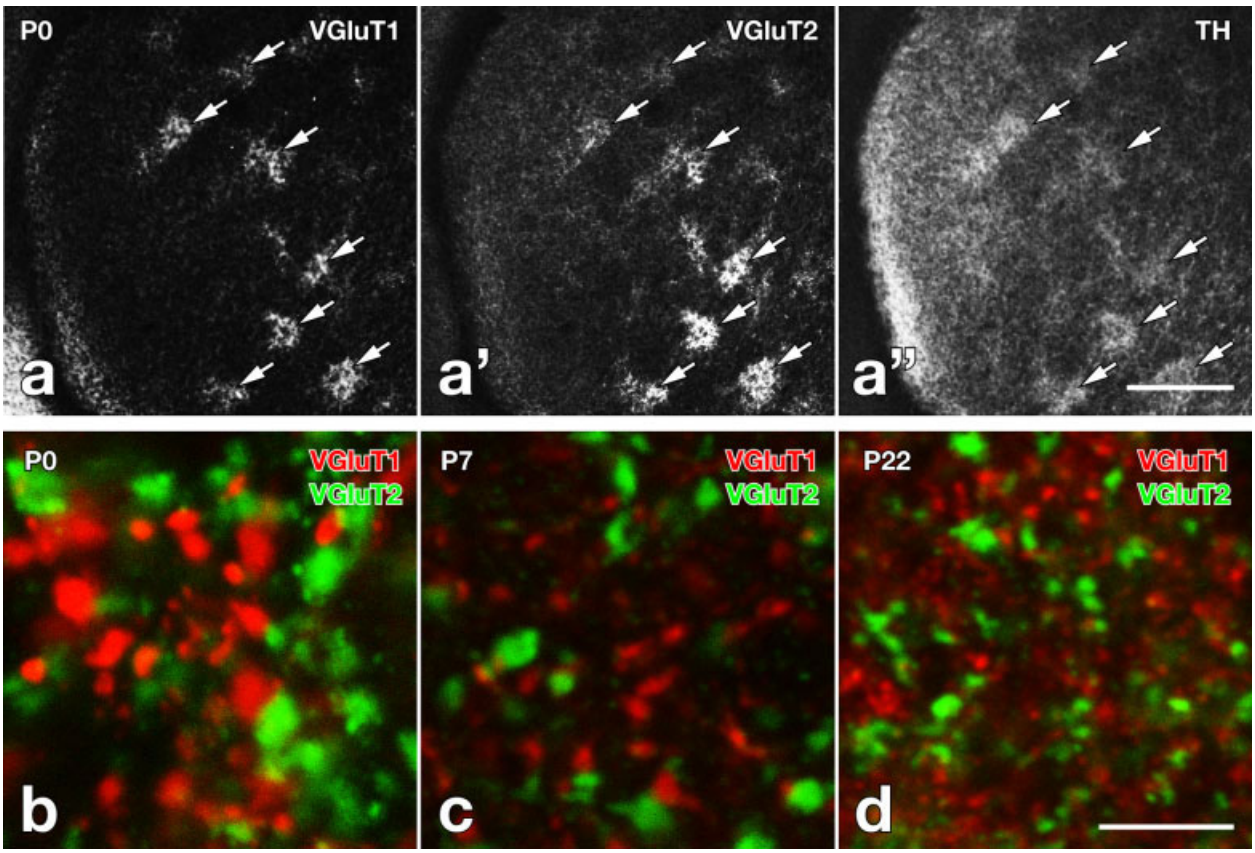


Fig. 7. VGluT1 and VGluT2 immunoreactivities in the postnatal developing caudate-putamen. **a–a′′:** Triple-immunofluorescence staining for VGluT1 (a; Cy5), VGluT2 (a′; Cy3), and tyrosine hydroxylase (TH, a′′; AlexaFluor 488) in the caudate-putamen of P0 mouse. Note that intensely immunoreactive regions in VGluT1- and VGluT2-immunolabeled sections correspond well to intensely TH-immunoreactive patches (arrows). The digital images were captured by a confocal laser-scanning microscope, LSM5 PASCAL, with maximum optical slice thickness. **b–d:** Confocal laser-scanning microscopic images (with optical slice thickness of less than 1.0 μm) of double-immunofluorescence staining for VGluT1 (red) and VGluT2 (green) in the caudate-putamen at P0 (b), P7 (c), and P22 (d) revealed that immunoreactivities for the two VGluTs were not colocalized in patch regions (b,c) or matrix region (d) of the caudate-putamen. For abbreviations, see list. Scale bars = 200 μm in a′′(applies to a–a′′); 5 μm in d (applies to b–d).

whereas VGluT2 immunoreactivity was weak. Immunoreactivities for the two VGluTs progressively increased in the matrix and decreased in the patches during the first postnatal week (Fig. 2a–e′). VGluT1 immunoreactivity became almost homogeneous between the patches and matrix after P10 (Fig. 2f–h), whereas VGluT2 immunoreactivity became slightly more intense in the matrix than in the patches after P10 (Fig. 2f′–h′). VGluT2 immunoreactivity of the patches decreased earlier in the dorsal region of the caudate-putamen than in the ventral region during the second postnatal week (Fig. 2e′–g′). In the double-immunofluorescence analysis, VGluT1 and VGluT2 immunoreactivities were not colocalized at single putative axon terminals of the caudate putamen, even in the patches, throughout postnatal development (patches, Fig. 7b,c; matrix, Fig. 7d).

The accumbens nucleus of P0 mice showed very weak VGluT1 immunoreactivity and almost negative VGluT2 immunoreactivity. VGluT1 immunoreactivity was weak to moderate at P7 and moderate after P10, whereas VGluT2 immunoreactivity more clearly increased and became moderate to intense by P7 in the accumbens nucleus. The external and internal segments of the globus pallidus showed weak VGluT1 immunoreactivity throughout postnatal development, and VGluT2 immunoreactivity was weak at P0, slightly increased, and became weak to moderate by P5. In the subthalamic nucleus, VGluT1 immunoreactivity was very weak at P0, gradually increased, and became weak to moderate after P7, whereas VGluT2 immunoreactivity was very weak at P0 and became moderate by P10.

## Dorsal thalamus

VGluT2 immunoreactivity in most nuclei of the dorsal thalamus was weak at P0 and progressively increased during postnatal development (Figs. 2i′–p′, 8a′–m′). In the anterodorsal, anteroventral, and dorsal lateral geniculate (LGd) nuclei, VGluT2 immunoreactivity was very weak at P0 and intense after P7 (Fig. 8a′,c′,d′,f′,h′,j′,l′). The laterodorsal, lateroposterior, ventrolateral, mediodorsal, midline, and reticular nuclei showed weak VGluT2 immunoreactivity from P0 to P1 and moderate VGluT2 immunoreactivity after P5 (Fig. 8a′–d′,f′–h′,j′–l′). VGluT2 immunoreactivity in the posterior nuclei was weak from P0 to P1, moderate from P5 to P10, and weak at P22 (Fig. 8d′,h′,l′). The ventroanterior nucleus was

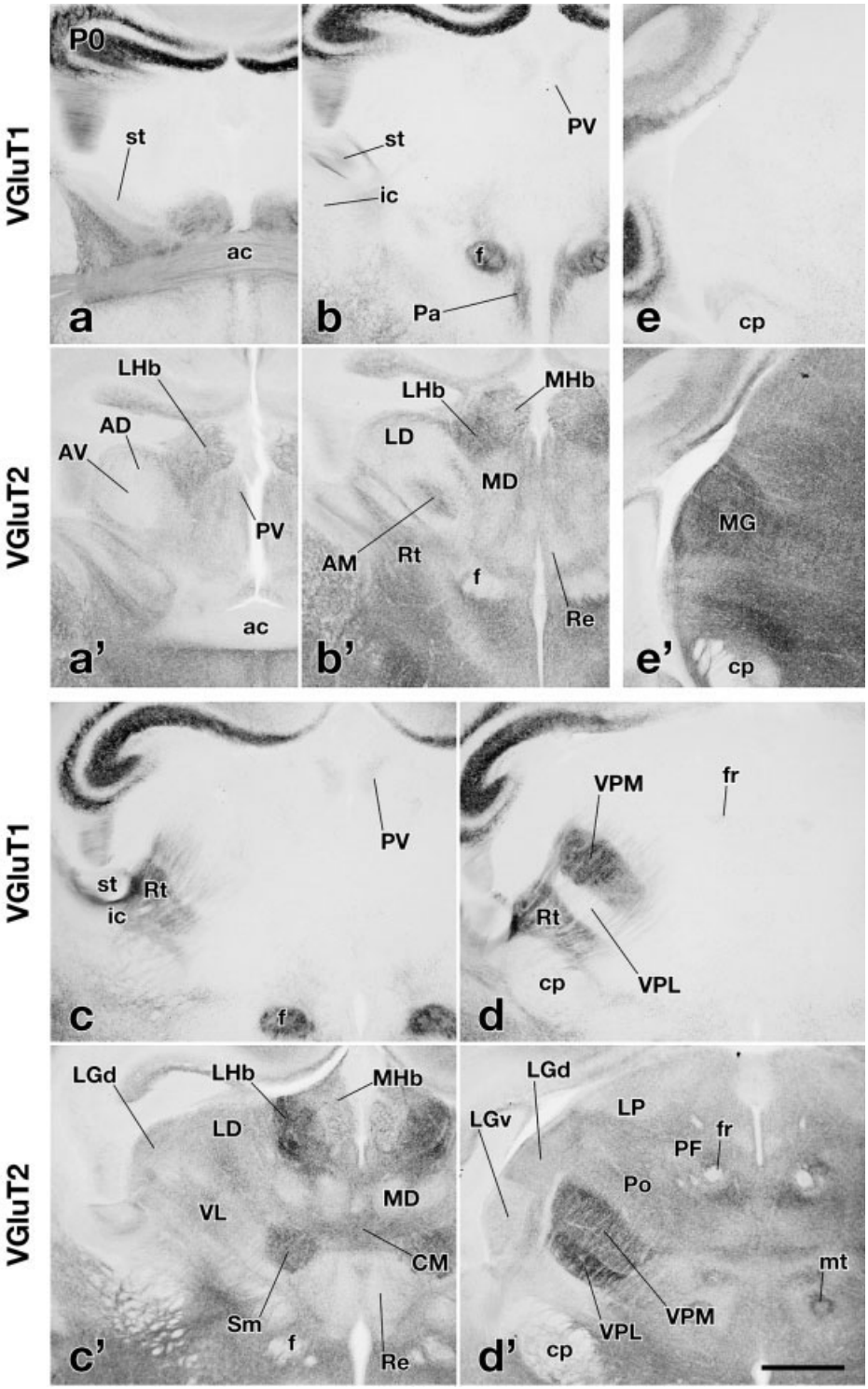


Fig. 8. VGluT1 and VGluT2 immunoreactivities in the postnatal developing thalamus at P0 (**a–e′**), P7 (**f–i′**), and P22 (**j–m′**). A letter and a letter with a prime sign indicate consecutive sections immunostained for VGluT1 and VGluT2, respectively. For abbreviations, see list. Scale bars = 500 μm in d′,i′,m′ (applies to a–m′′).

almost negative for VGluT2 until P1 and showed weak VGluT2 immunoreactivity after P3 (Fig. 8c′,g′,k′). The rest of the thalamic nuclei, however, showed weak to moderate or more VGluT2 immunoreactivity at P0. VGluT2 immunoreactivity of the anteromedial and intralaminar nuclei was weak to moderate from P0 to P1

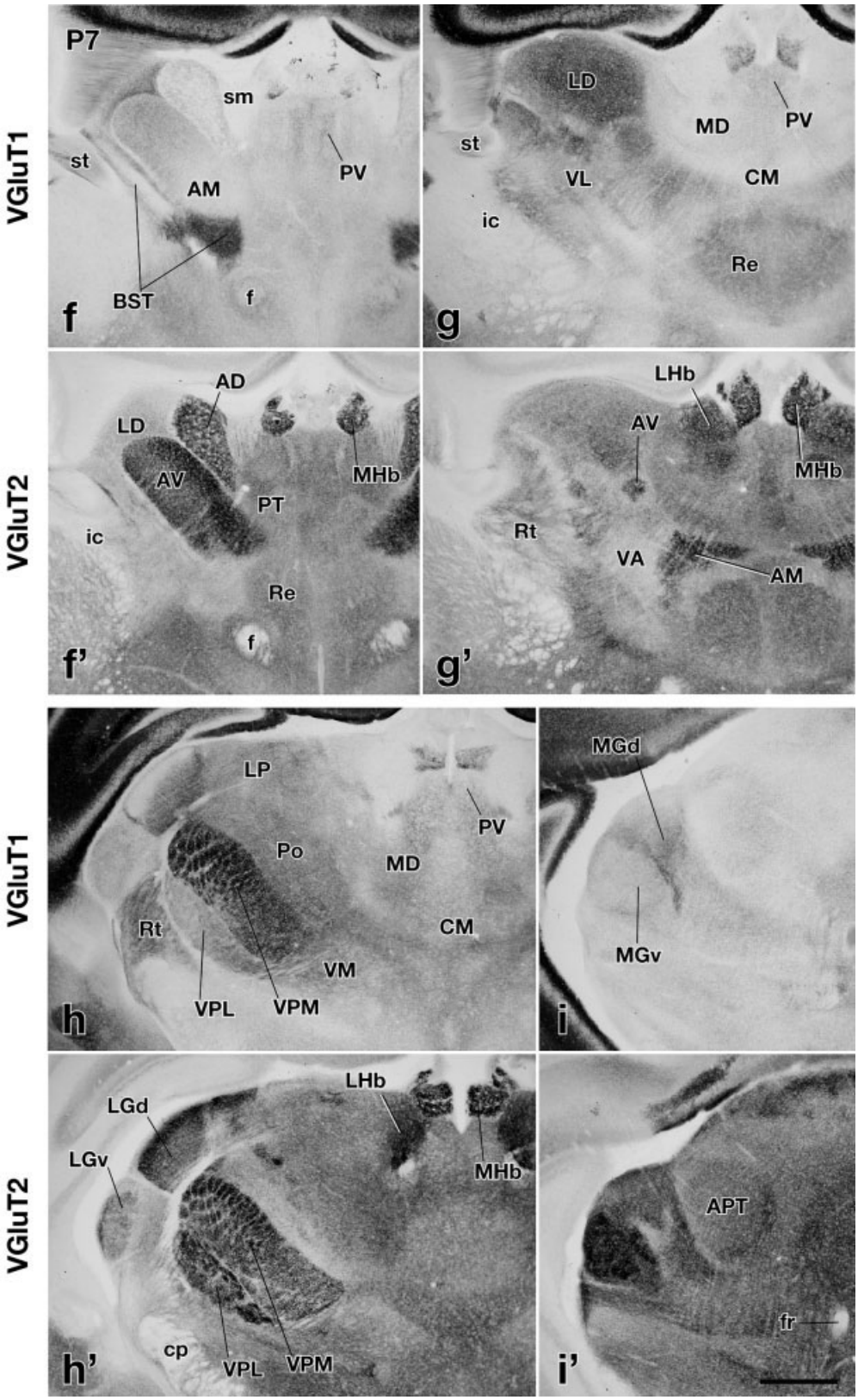


Figure 8 (Continued)

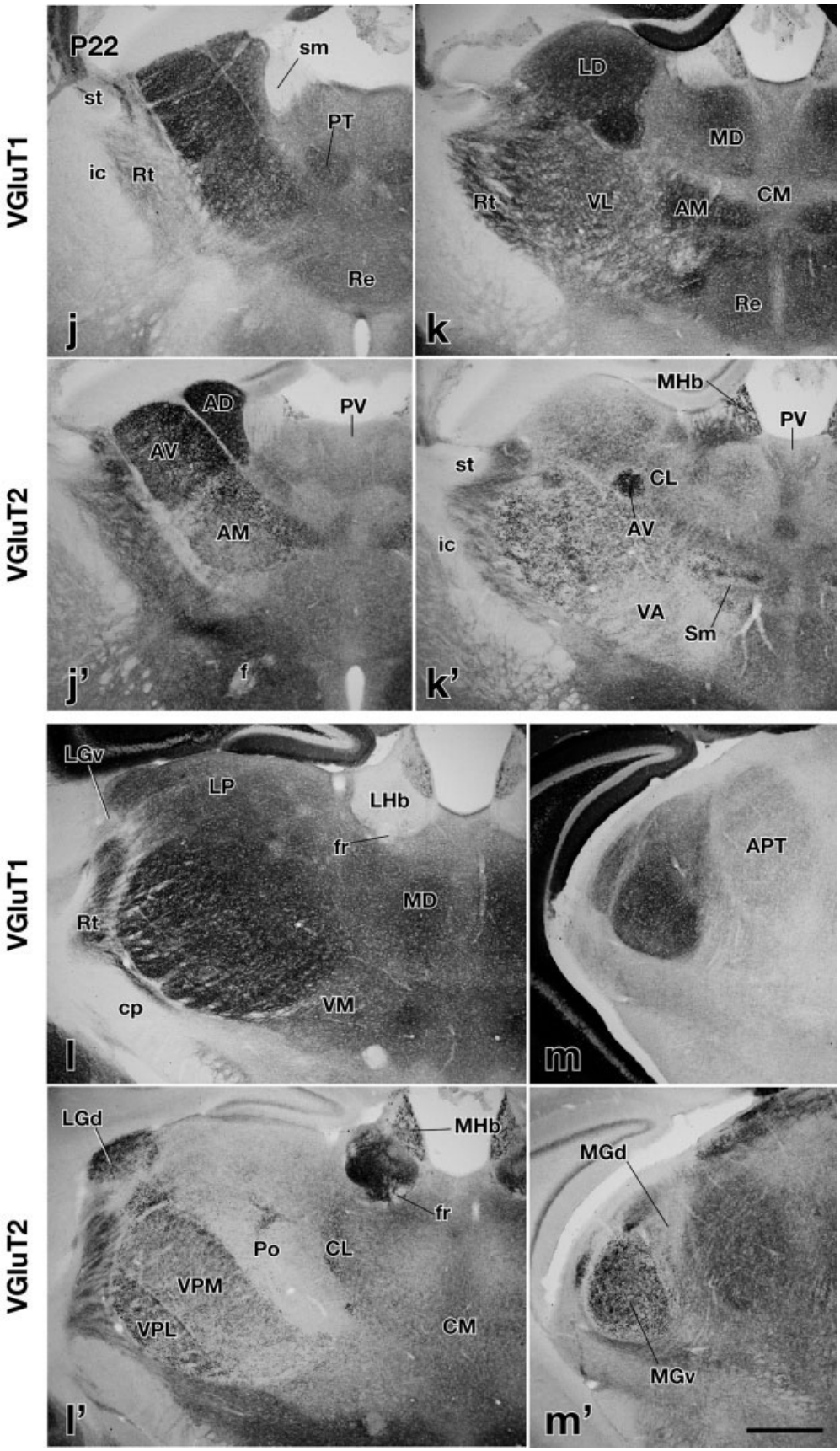


Figure 8 (Continued)

and moderate after P5 (Fig. 8b′–d′,f′–h′,j′–l′). The medial geniculate nucleus displayed moderate VGluT2 immunoreactivity at P0 and moderate to intense VGluT2 immunoreactivity after P5 (Fig. 8e′,i′,m′). In the ventral posteromedial (VPM) and ventral posterolateral (VPL) nuclei, VGluT2 immunoreactivity was moderate from P0 to P1, intense from P5 to P7, and weak to moderate from P14 to P22 (Figs. 2i′–p′, 8d′,h′,l′). Although, in the VPM and VPL, VGluT2 immunoreactivity was intense at each puncta and VGluT2-immunoreactive punctae increased in size from P7 to P14, VGluT2-immunoreactive punctae became more sparsely distributed during this period, resulting in an apparent decrease in VGluT2 immunoreactivity.

VGluT1 immunoreactivity was almost negative at P0 in most nuclei of the dorsal thalamus and showed a more marked increase during postnatal development than VGluT2 immunoreactivity (Figs. 2i–p, 8a–m). VGluT1 immunoreactivity in the anterior nuclei was negative until P1, very weak to weak from P3 to P5, and moderate by P14 (Fig. 8a,b,f,g,j,k). In the laterodorsal and lateroposterior nuclei, VGluT1 immunoreactivity was negative until P1, weak at P3, and moderate after P10 (Fig. 8b–d,g,h,k,l). In the mediodorsal, ventroanterior, and ventrolateral nuclei, VGluT1 immunoreactivity was negative by P1, very weak to weak at P3, and weak to moderate by P10 (Fig. 8b,c,g,h,k,l). VGluT1 immunoreactivity in the intralaminar and midline nuclei was negative at P0, very weak at P3, and weak to moderate by P10 (Fig. 8a–d,f–h,j–l). In the LGd and medial geniculate nucleus, VGluT1 immunoreactivity was negative until P1, very weak to weak from P3 to P7, and weak to moderate after P10 (Fig. 8c–e,h,i,l,m). VGluT1 immunoreactivity in the posterior nuclei was negative at P0, weak from P1 to P5, and moderate to intense after P14 (Fig. 8d,h,l). In the VPL, VGluT1 immunoreactivity was negative from P0 to P3, weak from P5 to P7, and moderate to intense after P14 (Fig. 8d,h,l).

Of the thalamic nuclei, only the reticular nucleus and VPM showed VGluT1 immunoreactivity as early as P0 (Fig. 8a–e). In the reticular nucleus, VGluT1 immunoreactivity was weak to moderate at P0 and P1 and moderate after P3 (Fig. 8d,h,l). VGluT1 immunoreactivity in the VPM was weak to moderate at P0 and P1 and moderate to intense after P3 (Figs. 2i–p, 8d,h,l). At P7, VGluT1 immunoreactivity in the VPM was distinctly higher than that in the VPL and was highest in the thalamus.

Double-immunofluorescence staining revealed frequent colocalization of VGluT1 and VGluT2 immunoreactivities at single putative axon terminals in the VPM from P0 to P7 (arrows, Fig. 9a–b′′). From P0 to P7, the size of the double-immunoreactive punctae was similar to that of punctae immunoreactive for VGluT1 or VGluT2 alone. From P10 to P14, colocalization of VGluT1 and VGluT2 immunoreactivities was also frequently found in the VPM, and punctae immunoreactive for both the VGluTs were larger in size than those immunoreactive for VGluT1 alone. Although we still found colocalization of immunoreactivities for both VGluTs in the VPM at P22 (Fig. 9e–e′′) and even in adulthood, VGluT1 immunoreactivity in VGluT2-immunoreactive large punctae was weak and did not fill the punctae (arrows, Fig. 9e–e′′). Instead, many small punctae were intensely immunoreactive for VGluT1 alone after P22. In contrast to the VPM, no colocalization of VGluT1 and VGluT2 immunoreactivities was found in the VPL (Fig. 9c–c′′) and LGd (Fig. 9d–d′′) throughout postnatal development, indicating that the colocalization of VGluT1 and VGluT2 immunoreactivities in the dorsal thalamus was restricted to the VPM.

### Epithalamus, preoptic regions, and hypothalamus

VGluT1 immunoreactivity in the lateral habenular nucleus was very weak to weak throughout postnatal development, whereas VGluT1 immunoreactivity in the medial habenular nucleus was very weak at P0, weak to moderate at P7, and moderate after P10 (Fig. 8a–c,f–h,k,l). VGluT2 immunoreactivity was moderate to intense in the lateral and medial habenular nuclei throughout postnatal development (Fig. 8a′–c′,f′–h′,k′,l′). In the fasciculus retroflexus, weakly to moderately VGluT1-immunoreactive fibers were observed throughout postnatal development. In good agreement with the present result, the previous in situ hybridization histochemical studies reported high levels of VGluT1 mRNA expression in the medial habenular nucleus (Fremeau et al., 2001; Herzog et al., 2001), suggesting that output from the medial habenular nucleus through the fasciculus retroflexus may include some glutamatergic fibers, although most axons in the tract were believed to be cholinergic.

In the preoptic region, VGluT1 immunoreactivity was very weak before P5 and weak after P10. VGluT2 immunoreactivity was weak in the medial preoptic area, moderate in the lateral preoptic area at P0, and, in both areas, progressively increased and became moderate to intense by P14. Although VGluT1 immunoreactivity in most hypothalamic regions was negative or very weak at P0, the paraventricular hypothalamic nucleus displayed weak to moderate VGluT1 immunoreactivity in the neuropil (Fig. 8b). The neuropil immunoreactivity in the paraventricular hypothalamic nucleus decreased and became very weak by P5. The ventromedial hypothalamic nucleus showed weak VGluT1 immunoreactivity from P3 to P7 and weak to moderate VGluT1 immunoreactivity after P10 (Fig. 2m–p). The mammillary nuclei showed very weak VGluT1 immunoreactivity at P0 and moderate VGluT1 immunoreactivity after P5 (Fig. 2q–x). VGluT2 immunoreactivity in the paraventricular hypothalamic nucleus, dorsal and lateral hypothalamic nucleus, and ventromedial hypothalamic nucleus was weak to moderate at P0, whereas VGluT2 immunoreactivity in the other hypothalamic nuclei including mammillary nuclei was weak or very weak at P0. VGluT2 immunoreactivity in hypothalamic nuclei progressively increased and became moderate to intense by P14 (Fig. 2i′–p′). In the mammillothalamic tract, weakly to moderately VGluT2-immunoreactive fibers were observed throughout postnatal development (Fig. 2i′–p′).

## DISCUSSION

In the present study, we first described developmental changes of VGluT1 and VGluT2 immunoreactivities in the mouse forebrain during the postnatal period. Neonatal forebrains were characterized by the early establishment of VGluT1 immunoreactivity in most limbic regions and by the predominant presence of VGluT2 immunoreactivity in diencephalic regions. This was followed by a rapid increase in VGluT1 immunoreactivity in the neocortical and diencephalic regions during 2 postnatal weeks. These immunocytochemical findings were almost compatible with

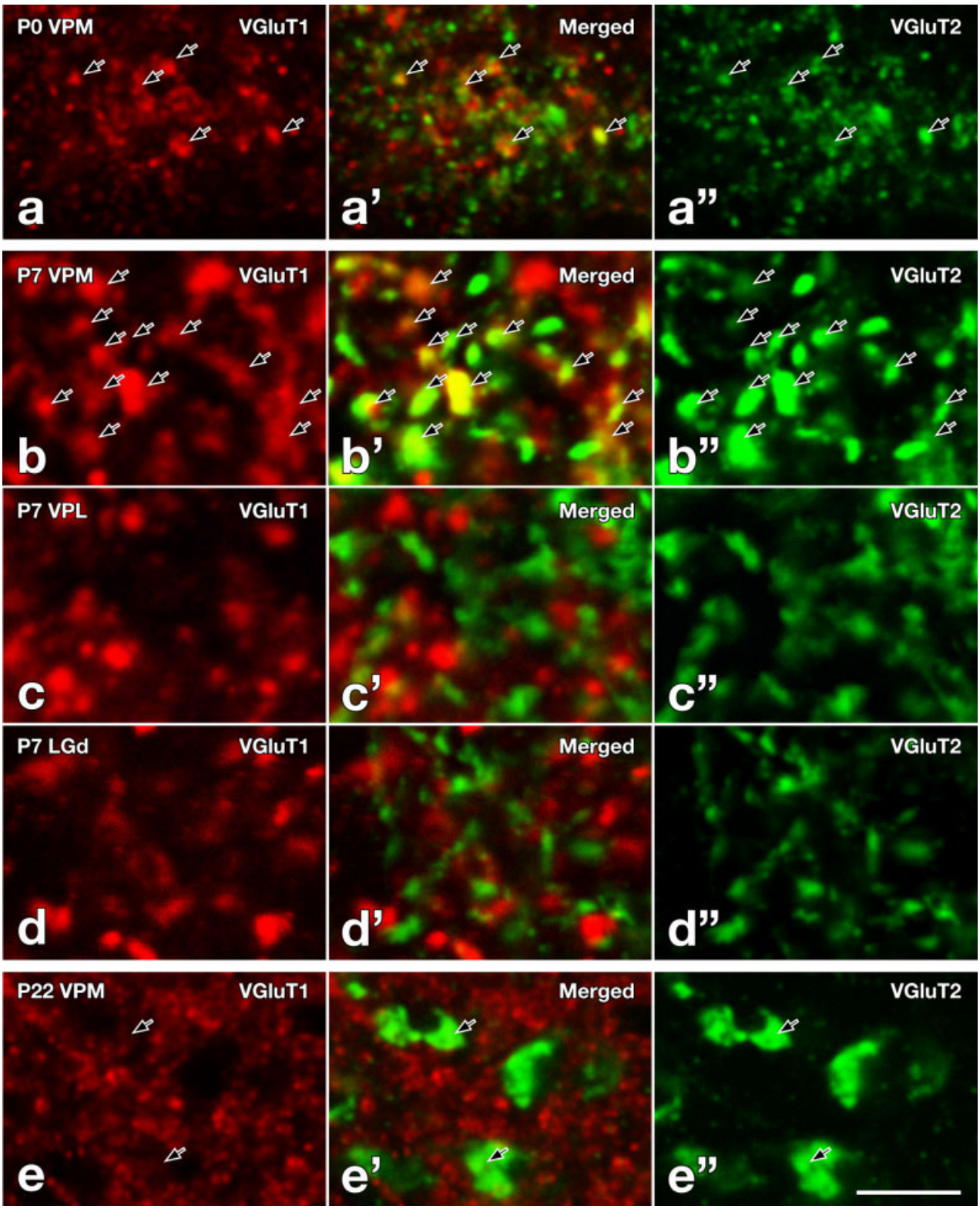


Fig. 9. Confocal laser-scanning microscopic analysis of double-immunofluorescence staining for VGluT1 (red) and VGluT2 (green) in the postnatal developing thalamus. **a–a′′:** In the ventral posteromedial nucleus (VPM) at P0, VGluT1 and VGluT2 immunoreactivities were frequently colocalized in small punctae (arrows). **b–d′′:** At P7, frequent colocalization of VGluT1 and VGluT2 immunoreactivities was observed in the VPM (arrows in b–b′′). In contrast, neither the ventral posterolateral thalamic nucleus (VPL, c–c′′) nor the dorsal lateral geniculate nucleus (LGd, d–d′′) showed such colocalization. **e–e′′:** Very weak VGluT1 immunoreactivity was still observed in VGluT2-immunoreactive large punctae in the VPM at P22 (arrows). For abbreviations, see list. Scale bars = 5 μm in e′′ (applies to a–e′′).

the recent immunoblotting and immunocytochemical results in developing rat brains (Boulland et al., 2004). We then, in the double-immunofluorescence studies, observed transient colocalization of VGluT1 and VGluT2 immunoreactivities during the postnatal period at single putative axon terminals in layer Ia of the piriform cortex, the barrel hollows of area S1, the stratum lucidum of hippocampal CA3 region, and the VPM.

## Technical considerations

Quantitative or semiquantitative analysis is necessary to evaluate developmental changes in immunoreactivity and its distribution. Immunoperoxidase staining sometimes shows fluctuations in intensity even under the same experimental conditions, and the fluctuations may be caused by differences in several processes, such as fixation, incubation, and enzymatic reaction for visualization. Thus, it is often difficult to quantitate and compare immunoreactivity precisely from animal to animal, or from region to region. In the present study, we tried to compare VGluT immunoreactivity in the brain tissues as carefully as possible by applying internal standards for VGluT immunoreactivity using some P22 mouse brain sections. Furthermore, whenever brain sections of any age were immunostained, we processed, in single incubation wells, a few P22 mouse sections containing the internal standard regions together with the brain sections of those ages and determined relative immunoreactivity in any brain region of a certain age by comparing it with immunoreactivity for the internal standard regions of P22 mice (Fig. 1a–f). The present semiquantitative results were in good agreement with quantitative immunoblotting findings of rat brain; VGluT1 displayed a dramatic increase in immunoreactivity in the cerebral cortex (Minelli et al., 2003) and in the whole brain (Boulland et al., 2004), and VGluT2 showed a less prominent increase during postnatal development in the whole brain (Boulland et al., 2004).

Detectability of the immunofluorescence methods is generally lower than that of the immunoperoxidase method with ABC. Because the low detectability often made us underestimate the colocalization of VGluT1 and VGluT2, we tried to enhance the immunofluorescence by increasing the concentration of the primary antibodies to 5 μg/ml. For further enhancement of immunofluorescence, we tested several antigen retrieval methods, such as protease treatment and heat treatment under various conditions. Heat treatment in weakly acidic and hypo-osmolar conditions (80°C, 10 mM citrate buffer, pH 6.0, 1 hour; Jiao et al., 1999) was most effective in enhancing immunoreactivities for both VGluT1 and VGluT2 (Fig. 1m–p). Thus, in the present immunofluorescence study, all sections were processed by heat treatment before immunostaining.

## VGluT1 immunoreactivity in the developing primary somatosensory area

In the adult rodent forebrains, VGluT1 and VGluT2 mRNAs are expressed predominantly in cortical pyramidal neurons and thalamic relay neurons, respectively (Fremeau et al., 2001; Herzog et al., 2001). VGluT1- and VGluT2-immunoreactive axon terminals in the cerebral cortex are thus considered to be mainly derived from pyramidal and thalamic relay neurons, respectively. This assumption was supported by the lesion experiment with kainic acid injection into the thalamic nuclei. VGluT2 immunoreactivity in the cerebral cortex corresponding to the injured thalamic nuclei was markedly decreased, whereas VGluT1 immunoreactivity was almost unchanged by the injection (Fujiyama et al., 2001). These results indicate that most VGluT2 immunoreactivity in the cerebral cortex is derived from the thalamic nuclei. Furthermore, Narhmani and Erisir (2005) recently reported that in layer IV of developing and adult ferret visual cortices most thalamocortical axon terminals labeled anterogradely with biotinylated dextran-amine showed VGluT2 but not VGluT1 immunoreactivity. Similar results were obtained in area S1 of adult rats when the thalamocortical afferents were labeled with an anterograde tracer, such as biotinylated dextran-amine and Sindbis virus vector with membrane-targeted green fluorescent protein (unpublished observations). Thus, at least in the adult cerebral cortex, little colocalization is expected between VGluT1 and VGluT2 immunoreactivities.

In the present developmental study, VGluT1 immunoreactivity was clearly observed in the hollows of the barrel cortex, suggesting that VGluT1 is located in the thalamocortical axon terminals. Actually, in the double-immunofluorescence staining, VGluT1 and VGluT2 immunoreactivities were frequently colocalized at single axon terminals in layer IV of P7 barrel cortex. Minelli et al. (2003) recently reported the postnatal development of VGluT1 immunoreactivity in rat area S1, and their results were largely consistent with the present findings on developmental changes. However, they did not describe clustering of moderately VGluT1-immunoreactive neuropil in the barrel hollows of P5 and P10 rat cortices. It is unlikely that this discrepancy is due to the difference in animal species, because in a preliminary study we observed similar VGluT1-immunoreactive barrel-like structures in P7 rat barrel cortex. Because we observed that barrel-like structures in VGluT1 immunoreactivity were much clearer in P7 mice (Fig. 2e) than in P5 or P10 mice, the discrepancy might be explained by the difference in postnatal ages analyzed. Moreover, the present observations were supported by recent in situ hybridization histochemical reports (Miyazaki et al., 2003; Fremeau et al., 2004b) in which VGluT1 mRNA signals were clearly detected in the developing mouse VPM. Thus, VGluT2-loaded thalamocortical axon terminals are considered to contain VGluT1 at least in P7 mouse barrel cortex.

In P22 and adult mouse brain, VGluT1 immunofluorescence was infrequently observed in VGluT2-positive axon terminals in layer IV of the barrel cortex. Because weak expression of VGluT1 mRNA in the thalamic nuclei including the VPM was reported even in adulthood (Ni et al., 1995; Fremeau et al., 2001, 2004b; Herzog et al., 2001; Miyazaki et al., 2003), the infrequent colocalization of VGluT1 and VGluT2 in adult barrel cortex might indicate that the present immunofluorescence method was still insufficient to detect such low levels of VGluT1 protein. In any case, the present results suggest that VGluT1 immunoreactivity increased transiently during the early postnatal period at thalamocortical axon terminals of the barrel cortex.

## VGluT1 and VGluT2 immunoreactivities in the developing hippocampus

In the molecular layer of the dentate gyrus, the present study showed that some VGluT1-immunoreactive punctae were positive for VGluT2 at P7 and in adulthood. In good

agreement with the present results, Boulland et al. (2004) reported that less than 10% of glutamatergic terminals in the molecular layer of adult rats showed both VGluT1 and VGluT2 immunoreactivities by immunogold electron microscopy. In the stratum radiatum of hippocampal CA1 region, Fremeau et al. (2004b) and we did not find colocalization of the two VGluTs by double-immunofluorescence staining of mouse sections. Boulland et al. (2004), however, reported that a subset (less than 10%) of glutamatergic terminals in the CA1 stratum radiatum of adult rats showed both VGluT1 and VGluT2 immunoreactivities by immunoelectron microscopy. This inconsistency might be accounted for by the difference in animal species.

Fremeau et al. (2004b) reported transient coexpression of VGluT1 and VGluT2 in single hippocampal pyramidal neurons of 1-week-old mice by in situ hybridization histochemistry and electrophysiology, and by means of MK-801-mediated progressive blockade of NMDA currents in VGluT1 knockout mice, they also showed that the coexpressed VGluT1 and VGluT2 were targeted to distinct release sites of single neurons. In the present study, colocalization of VGluT1 and VGluT2 immunoreactivities was not transient but was observed even after P22 in the stratum lacunosum-moleculare of Ammon's horn. It is thus likely that those terminals immunoreactive for both the VGluTs were not derived from hippocampal pyramidal neurons. The reuniens thalamic nucleus has been reported to send axons into the stratum lacunosum-moleculare of CA1 (Wouterlood et al., 1990) and to show both VGluT1 and VGluT2 mRNA signals in adult rats (Collin et al., 2003). The VGluT1 and VGluT2 double-immunoreactive axon terminals in the stratum lacunosum-moleculare may thus be derived from the reuniens thalamic nucleus.

The present study showed that large VGluT1-immunoreactive punctae were transiently immunoreactive for VGluT2 from P5 to P14 in the stratum lucidum of CA3 and the hilar region of the dentate gyrus. The VGluT1-immunoreactive large punctae in the stratum lucidum and hilus were assumed to be mossy fiber terminals from granule cells of the dentate gyrus, because it was reported that granule cells expressed VGluT1 mRNA (Fremeau et al., 2001; Herzog et al., 2001) and that mossy fiber terminals were large (3–6 μm in diameter) in the stratum lucidum of CA3 and the hilar region of the dentate gyrus (Shepherd, 2004). Thus, the transient colocalization of VGluT2 immunoreactivity at large VGluT1-immunoreactive punctae in the stratum lucidum and dentate hilus of developing mice was in good agreement with the finding that VGluT2 mRNA was transiently expressed in granule cells of the developing dentate gyrus (Miyazaki et al., 2003).

## VGluT1 and VGluT2 immunoreactivities in the developing caudate-putamen

In the caudate-putamen, VGluT1 and VGluT2 immunoreactivities were not colocalized at single axon terminals in either the patches or matrix at any postnatal days analyzed. It has been reported that in adult rat caudate-putamen VGluT1- and VGluT2-immunoreactive terminals are derived from the neocortex and thalamus, respectively (Fujiyama et al., 2004). No occurrence of colocalization during development suggests that the specificity of VGluT isoform expression in the two major excitatory inputs may have begun in the early postnatal period.

During the first postnatal week, both VGluT1 and VGluT2 immunoreactivities were more intense in the patches than in the matrix, indicating that most glutamatergic inputs were confined to the patch regions during this period. Neurons in the patches have been reported to be generated approximately 5 days earlier than those in the matrix (van der Kooy et al., 1987). It has been reported that several glutamate receptors, such as mGluR1alpha, GluR1, GluR2/3, NMDAR1, and NMDAR2A/2B, are expressed predominantly in neurons of the patches at P0 (Snyder-Keller et al., 1996; Jokel et al., 2001). Furthermore, striatonigral projections are established first by neurons in the patches around birth, much earlier than by neurons in the matrix (Fishell and van der Kooy, 1987). These findings as well as the present results suggest that neurons and their circuitry in the patch regions mature earlier than those in the matrix.

## Colocalization of VGluT1 and VGluT2 immunoreactivities in the developing ventral posteromedial thalamic nucleus

Of the thalamic nuclei, immunoreactivity for VGluT1 was prominent almost exclusively in the VPM throughout the first postnatal week, whereas VGluT2 immunoreactivity was moderate to intense in both the VPM and VPL during the same period. At P22, however, VGluT1 immunoreactivity was moderate to intense in both the VPM and VPL. Moreover, the VPM of P0–P14 mice showed frequent colocalization of intense VGluT1 and VGluT2 immunoreactivities at single axon terminals, but the colocalization became infrequent after P22.

The VGluT1 and VGluT2 double-immunoreactive terminals observed transiently in the VPM could be derived from three possible sources: thalamic relay neurons, neocortical pyramidal neurons, or trigeminal neurons. Relay neurons in the VPM, however, have no axon collaterals within the nucleus (for review, see Shepherd, 2004), and it is thus unlikely that the VGluT1 and VGluT2 double-immunoreactive terminals in the VPM were derived from the relay neurons. Corticothalamic axon terminals were also unlikely to show VGluT2 immunoreactivity, because VGluT2 mRNA was not detected in deep layers of developing mouse cortex (Miyazaki et al., 2003; Fremeau et al., 2004b). Thus, trigeminal ascending inputs were the only possible source of VGluT1 and VGluT2 double-immunoreactive terminals in the VPM. This possibility is supported by the observation that the double-immunoreactive punctae were much larger than punctae immunoreactive only for VGluT1 in the VPM of P10 mice, because the corticothalamic terminals are generally much smaller than ascending afferent terminals in the thalamic nuclei (for review, see Shepherd, 2004).

## Functional significance of transient colocalization of VGluT1 and VGluT2 immunoreactivities

VGluT1 and VGluT2 have been reported to possess very similar biochemical and pharmacological characteristics for accumulating neurotransmitter glutamate into synaptic vesicles (for review, see Kaneko and Fujiyama, 2002) except that the composition of heterotrimeric G-protein subunits was different between VGluT1- and VGluT2-

laden axon terminals (Pahner et al., 2003). However, VGluT2-laden synapses, such as retinogeniculate synapses and those between cerebellar climbing fibers and Purkinje cells, have been demonstrated to show synaptic depression (Turner and Salt, 1998; Dittman et al., 2000); when the synapses are activated repeatedly, the second synaptic response is smaller than the first one. In contrast, VGluT1-loaded corticothalamic synapses and parallel fiber-Purkinje cell synapses are known to display synaptic facilitation (Deschênes and Hu, 1990; Lindström and Wróbel, 1990; Turner and Salt, 1998; Von Krosgik et al., 1999; Dittman et al., 2000). Depressing synapses are considered to be suitable for high-fidelity transmission of information, whereas facilitating synapses seem to be utilized for integration and/or high-pass filtering of information. Moreover, VGluT1-positive synapses often showed long-term synaptic plasticity, such as long-term depression in cerebellar parallel fiber-Purkinje cell synapses (Ito and Kano, 1982) and long-term potentiation in corticothalamic synapses (Castro-Alamancos and Calcagnotto, 1999). Thus, these facts strongly point out that the two isoforms of VGluTs may be related to distinct functional characteristics of excitatory synapses and suggest that VGluT1 is more associated with synapses showing plasticity than VGluT2.

Thalamocortical synapses of rat barrel cortex have been reported to show long-term synaptic plasticity only during the first postnatal week in rats (for review, see Feldman et al., 1999), suggesting that the thalamocortical synapses might mature within a week after birth. However, Yanagisawa et al. (2004) very recently reported that paired-pulse synaptic depression of excitatory thalamocortical response was not observed at P4 and progressively increased until P22 in layer IV of mouse barrel cortex. Because the synaptic properties characterized by synaptic depression or facilitation are considered to be mainly determined by the presynaptic mechanisms (for review, see Thomson, 2000), the thalamocortical synapses of rodent barrel cortex may still be immature at least in their presynaptic components during the first 3 weeks after birth. In the present study, we revealed the transient coexistence of VGluT1 immunoreactivity at VGluT2-immunoreactive thalamocortical axon terminals in P5–P10 barrel cortex. Because many VGluT1-loaded synapses show synaptic facilitation, as discussed above, the presence of VGluT1 at VGluT2-laden thalamocortical terminals might suppress synaptic depression during the early postnatal period.

In addition to the thalamocortical axon terminals in the barrel cortex, trigeminothalamic terminals in the VPM appeared to use both VGluT1 and VGluT2 in the early postnatal period. This finding is in sharp contrast to observations in the VPL, where no VGluT1 immunoreactivity was detected in putative lemniscal and spinothalamic afferent terminals that were immunoreactive for VGluT2. This striking contrast between the two somatosensory systems, trigeminal and lemniscal/spinothalamic, suggests their distinct characteristics during postnatal development. It has been reported that immunoreactivity for neurotrophin receptor p75 is not seen in the VPL but is transiently observed in the VPM from the prenatal period to P13 in developing rats (Crockett et al., 2000), showing differences between the two somatosensory systems in postnatal development. This observation, together with the present results, suggests that the trigeminal system in rodents may have different synaptic characteristics from the lemniscal/spinothalamic system in early postnatal development, including the so-called critical period.

## ACKNOWLEDGMENTS

The authors thank Dr. Takahiro Furuta for helpful discussion.

## LITERATURE CITED

Altman J, Bayer SA. 1995. Atlas of prenatal rat brain development. Boca Raton: CRC Press.

Bai L, Xu H, Collins JF, Ghishan FK. 2001. Molecular and functional analysis of a novel neuronal vesicular glutamate transporter. J Biol Chem 276:36764–36769.

Bellocchio EE, Hu H, Pohorille A, Chan J, Pickel VM, Edwards RH. 1998. The localization of the brain-specific inorganic phosphate transporter suggests a specific presynaptic role in glutamatergic transmission. J Neurosci 18:8648–8659.

Bellocchio EE, Reimer RJ, Fremeau RT Jr, Edwards RH. 2000. Uptake of glutamate into synaptic vesicles by an inorganic phosphate transporter. Science 289:957–960.

Boulland JL, Qureshi T, Seal RP, Rafiki A, Gundersen V, Bergersen LH, Fremeau RT Jr, Edwards RH, Storm-Mathisen J, Chaudhry FA. 2004. Expression of the vesicular glutamate transporters during development indicates the widespread corelease of multiple neurotransmitters. J Comp Neurol 480:264–280.

Broman J, Hassel B, Rinvik E, Ottersen OP. 2000. Biochemistry and anatomy of transmitter glutamate. In: Ottersen OP, Storm-Mathisen J, editors. Handbook of chemical neuroanatomy, vol. 18. Glutamate. Amsterdam: Elsevier. p 1–44.

Castro-Alamancos MA, Calcagnotto ME. 1999. Presynaptic long-term potentiation in corticothalamic synapses. J Neurosci 19:9090–9097.

Collin M, Bäckberg M, Ovesjö ML, Fisone G, Edwards RH, Fujiyama F, Meister B. 2003. Plasma membrane and vesicular glutamate transporter mRNAs/proteins in hypothalamic neurons that regulate body weight. Eur J Neurosci 18:1265–1278.

Crockett DP, Harris SL, Egger MD. 2000. Neurotrophin receptor (p75) in the trigeminal thalamus of the rat: development, response to injury, transient vibrissa-related patterning, and retrograde transport. Anat Rec 259:446–460.

Deschênes M, Hu B. 1990. Electrophysiology and pharmacology of the corticothalamic input to lateral thalamic nuclei: an intracellular study in the cat. Eur J Neurosci 2:140–152.

Dittman JS, Kreitzer AC, Regehr WG. 2000. Interplay between facilitation, depression, and residual calcium at three presynaptic terminals. J Neurosci 20:1374–1385.

Feldman DE, Nicoll RA, Malenka RC. 1999. Synaptic plasticity at thalamocortical synapses in developing rat somatosensory cortex: LTP, LTD, and silent synapses. J Neurobiol 41:92–101.

Fishell G, van der Kooy D. 1987. Pattern formation in the striatum: developmental changes in the distribution of striatonigral neurons. J Neurosci 7:1969–1978.

Fremeau RT Jr, Troyer MD, Pahner I, Nygaard GO, Tran CH, Reimer RJ, Bellocchio EE, Fortin D, Storm-Mathisen J, Edwards RH. 2001. The expression of vesicular glutamate transporters defines two classes of excitatory synapse. Neuron 31:247–260.

Fremeau RT Jr, Burman J, Qureshi T, Tran CH, Proctor J, Johnson J, Zhang H, Sulzer D, Copenhagen DR, Storm-Mathisen J, Reimer RJ, Chaudhry FA, Edwards RH. 2002. The identification of vesicular glutamate transporter 3 suggests novel modes of signaling by glutamate. Proc Natl Acad Sci U S A 99:14488–14493.

Fremeau RT Jr, Voglmaier S, Seal RP, Edwards RH. 2004a. VGLUTs define subsets of excitatory neurons and suggest novel roles for glutamate. Trends Neurosci 27:98–103.

Fremeau RT Jr, Kam K, Qureshi T, Johnson J, Copenhagen DR, Storm-Mathisen J, Chaudhry FA, Nicoll RA, Edwards RH. 2004b. Vesicular glutamate transporters 1 and 2 target to functionally distinct synaptic release sites. Science 304:1815–1819.

Fujiyama F, Furuta T, Kaneko T. 2001. Immunocytochemical localization of candidates for vesicular glutamate transporters in the rat cerebral cortex. J Comp Neurol 435:379–387.

Fujiyama F, Kuramoto E, Okamoto K, Hioki H, Furuta T, Zhou L, Nomura

S, Kaneko T. 2004. Presynaptic localization of an AMPA-type glutamate receptor in corticostriatal and thalamostriatal axon terminals. Eur J Neurosci 20:3322–3330.

Gerfen CR. 1992. The neostriatal mosaic: multiple levels of compartmental organization. Trends Neurosci 15:133–139.

Gras C, Herzog E, Bellenchi GC, Bernard V, Ravassard P, Pohl M, Gasnier B, Giros B, El Mestikawy S. 2002. A third vesicular glutamate transporter expressed by cholinergic and serotoninergic neurons. J Neurosci 22:5442–5451.

Graybiel AM, Pickel VM, Joh TH, Reis DJ, Ragsdale CW Jr. 1981. Direct demonstration of a correspondence between the dopamine islands and acetylcholinesterase patches in the developing striatum. Proc Natl Acad Sci U S A 78:5871–5875.

Hayar A, Karnup S, Ennis M, Shipley MT. 2004. External tufted cells: a major excitatory element that coordinates glomerular activity. J Neurosci 24:6676–6685.

Herlenius E, Lagercrantz H. 2004. Development of neurotransmitter systems during critical periods. Exp Neurol 190 Suppl 1:S8–21.

Herzog E, Bellenchi GC, Gras C, Bernard V, Ravassard P, Bedet C, Gasnier B, Giros B, El Mestikawy S. 2001. The existence of a second vesicular glutamate transporter specifies subpopulations of glutamatergic neurons. J Neurosci 21:RC181.

Hioki H, Fujiyama F, Taki K, Tomioka R, Furuta T, Tamamaki N, Kaneko T. 2003. Differential distribution of vesicular glutamate transporters in the rat cerebellar cortex. Neuroscience 117:1–6.

Hioki H, Fujiyama F, Nakamura K, Wu SX, Matsuda W, Kaneko T. 2004. Chemically specific circuit composed of vesicular glutamate transporter 3- and preprotachykinin B-producing interneurons in the rat neocortex. Cereb Cortex 14:1266–1275.

Hisano S, Hoshi K, Ikeda Y, Maruyama D, Kanemoto M, Ichijo H, Kojima I, Takeda J, Nogami H. 2000. Regional expression of a gene encoding a neuron-specific Na(+)-dependent inorganic phosphate cotransporter (DNPI) in the rat forebrain. Mol Brain Res 83:34–43.

Ito M, Kano M. 1982. Long-lasting depression of parallel fiber-Purkinje cell transmission induced by conjunctive stimulation of parallel fibers and climbing fibers in the cerebellar cortex. Neurosci Lett 33:253–258.

Jiao Y, Sun Z, Lee T, Fusco FR, Kimble TD, Meade CA, Cuthbertson S, Reiner A. 1999. A simple and sensitive antigen retrieval method for free-floating and slide-mounted tissue sections. J Neurosci Methods 93:149–162.

Jokel ES, Garduno ER, Ariano MA, Levine MS. 2001. Metabotropic glutamate receptors mGluR1alpha and mGluR2/3 display dynamic expression patterns in developing rat striatum. Dev Neurosci 23:1–6.

Kaneko T. 2000. Enzymes responsible for glutamate synthesis and degradation. In: Ottersen OP, Storm-Methisen J, editors. Handbook of chemical neuroanatomy, vol. 18. Glutamate. Amsterdam: Elsevier. p 203–230.

Kaneko T, Fujiyama F. 2002. Complementary distribution of vesicular glutamate transporters in the central nervous system. Neurosci Res 42:243–250.

Kaneko T, Mizuno N. 1988. Immunohistochemical study of glutaminase-containing neurons in the cerebral cortex and thalamus of the rat. J Comp Neurol 267:590–602.

Kaneko T, Mizuno N. 1992. Postnatal changes of glutaminase-like immunoreactivity in the olfactory bulb, thalamus, cerebral cortex and cerebellum of the rat. In: Björklund A, Hökfelt T, Tohyama M, editors. Handbook of chemical neuroanatomy, vol. 10. Ontogeny of transmitters and peptides in the CNS. Amsterdam: Elsevier. p 177–195.

Kaneko T, Mizuno N. 1994. Glutamate-synthesizing enzymes in GABAergic neurons of the neocortex: a double immunofluorescence study in the rat. Neuroscience 61:839–849.

Kaneko T, Nakaya Y, Mizuno N. 1992. Paucity of glutaminase-immunoreactive nonpyramidal neurons in the rat cerebral cortex. J Comp Neurol 322:181–190.

Kaneko T, Fujiyama F, Hioki H. 2002. Immunohistochemical localization of candidates for vesicular glutamate transporters in the rat brain. J Comp Neurol 444:39–62.

Lindström S, Wróbel A. 1990. Frequency dependent corticofugal excitation of principal cells in the cat's dorsal lateral geniculate nucleus. Exp Brain Res 79:313–318.

Luján R, Shigemoto R, López-Bendito G. 2005. Glutamate and GABA receptor signalling in the developing brain. Neuroscience 130:567–580.

Minelli A, Edwards RH, Manzoni T, Conti F. 2003. Postnatal development of the glutamate vesicular transporter VGLUT1 in rat cerebral cortex. Dev Brain Res 140:309–314.

Miyazaki T, Fukaya M, Shimizu H, Watanabe M. 2003. Subtype switching of vesicular glutamate transporters at parallel fibre-Purkinje cell synapses in developing mouse cerebellum. Eur J Neurosci 17:2563–2572.

Nahmani M, Erisir A. 2005. VGluT2 immunochemistry identifies thalamocortical terminals in layer 4 of adult and developing visual cortex. J Comp Neurol 484:458–473.

Ni B, Wu X, Yan GM, Wang J, Paul SM. 1995. Regional expression and cellular localization of the Na(+)-dependent inorganic phosphate cotransporter of rat brain. J Neurosci 15:5789–5799.

Pahner I, Höltje M, Winter S, Takamori S, Bellocchio EE, Spicher K, Laake P, Nürnberg B, Ottersen OP, Ahnert-Hilger G. 2003. Functional G-protein heterotrimers are associated with vesicles of putative glutamatergic terminals: implications for regulation of transmitter uptake. Mol Cell Neurosci 23:398–413.

Paxinos G, Franklin KBJ. 2001 The mouse brain in stereotaxic coordinates, 2nd ed. San Diego: Academic Press.

Paxinos G, Törk I, Tecott LH, Valentino KL. 1991. Atlas of the developing rat brain. San Diego: Academic Press.

Schäfer MK, Varoqui H, Defamie N, Weihe E, Erickson JD. 2002. Molecular cloning and functional identification of mouse vesicular glutamate transporter 3 and its expression in subsets of novel excitatory neurons. J Biol Chem 277:50734–50748.

Shepherd, GM. 2004. The synaptic organization of the brain, 5th ed. New York: Oxford University Press.

Snyder-Keller A, Costantini LC. 1996. Glutamate receptor subtypes localize to patches in the developing striatum. Dev Brain Res 94:246–250.

Takamori S, Rhee JS, Rosenmund C, Jahn R. 2000. Identification of a vesicular glutamate transporter that defines a glutamatergic phenotype in neurons. Nature 407:189–194.

Takamori S, Rhee JS, Rosenmund C, Jahn R. 2001. Identification of differentiation-associated brain-specific phosphate transporter as a second vesicular glutamate transporter (VGLUT2). J Neurosci 21: RC182.

Takamori S, Malherbe P, Broger C, Jahn R. 2002. Molecular cloning and functional characterization of human vesicular glutamate transporter 3. EMBO Rep 3:798–803.

Thomson AM. 2000. Facilitation, augmentation and potentiation at central synapses. Trends Neurosci 23:305–312.

Turner JP, Salt TE. 1998. Characterization of sensory and corticothalamic excitatory inputs to rat thalamocortical neurones in vitro. J Physiol 510:829–843.

van der Kooy D, Fishell G. 1987. Neuronal birthdate underlies the development of striatal compartments. Brain Res 401:155–161.

Varoqui H, Schäfer MK, Zhu H, Weihe E, Erickson JD. 2002. Identification of the differentiation-associated Na+/PI transporter as a novel vesicular glutamate transporter expressed in a distinct set of glutamatergic synapses. J Neurosci 22:142–155.

von Krosigk M, Monckton JE, Reiner PB, McCormick DA. 1999. Dynamic properties of corticothalamic excitatory postsynaptic potentials and thalamic reticular inhibitory postsynaptic potentials in thalamocortical neurons of the guinea-pig dorsal lateral geniculate nucleus. Neuroscience 91:7–20.

Wojcik SM, Rhee JS, Herzog E, Sigler A, Jahn R, Takamori S, Brose N, Rosenmund C. 2004. An essential role for vesicular glutamate transporter 1 (VGLUT1) in postnatal development and control of quantal size. Proc Natl Acad Sci U S A 101:7158–7163.

Wouterlood FG, Saldana E, Witter MP. 1990. Projection from the nucleus reuniens thalami to the hippocampal region: light and electron microscopic tracing study in the rat with the anterograde tracer *Phaseolus vulgaris*-leucoagglutinin. J Comp Neurol 296:179–203.

Yanagisawa T, Tsumoto T, Kimura F. 2004. Transiently higher release probability during critical period at thalamocortical synapses in the mouse barrel cortex: relevance to differential short-term plasticity of AMPA and NMDA EPSCs and possible involvement of silent synapses. Eur J Neurosci 20:3006–3018.